SIAM J. Applied Dynamical Systems
Vol. 2, No. 1, pp. 53–96

Semistrong Pulse Interactions in a Class of Coupled Reaction-Diffusion Equations*

Arjen Doelman† and Tasso J. Kaper‡

This article is dedicated in memory of Wiktor Eckhaus.

Abstract. Pulse-pulse interactions play central roles in a variety of pattern formation phenomena, including self-replication. In this article, we develop a theory for the semistrong interaction of pulses in a class of singularly perturbed coupled reaction-diffusion equations that includes the (generalized) Gierer–Meinhardt, Gray–Scott, Schnakenberg, and Thomas models, among others. Geometric conditions are determined on the reaction kinetics for whether the pulses in a two-pulse solution attract or repel, and ODEs are derived for the time-dependent separation distance between their centers and for their wave speeds. In addition, conditions for the existence of stationary two-pulse solutions are identified, and the interactions between stationary and dynamically evolving two-pulse solutions are studied. The theoretical results are illustrated in a series of examples. In two of these, which are related to the classical Gierer–Meinhardt equation, we find that the pulse amplitudes blow up in finite time. Moreover, the blowup of stationary one-pulse solutions and of dynamically varying two-pulse solutions occurs precisely at the parameter values for which the theory we develop predicts that these solutions should cease to exist as bounded solutions. Finally, generalizations to N-pulse solutions are presented.

Key words. reaction-diffusion equations, semistrong pulse interactions, multipulse traveling waves, geometric singular perturbation theory, finite-time blowup, self-replicating pulses

AMS subject classifications. 35K57, 35K45, 35B25, 35B32, 35B40, 34C30, 34C37, 92E20

PII. S1111111102405719

1. Introduction.

In this article, we study the semistrong interaction of pulses in a general class of coupled reaction-diffusion equations in one spatial dimension. The focus is on pattern formation in far-from-equilibrium systems in which the pulses are localized large-amplitude perturbations of a linearly stable, homogeneous, background state. The label semistrong signifies that the concentration of one of the species is far from equilibrium on the domain between the pulse centers, and hence the pulse interaction is governed to leading order through the slow spatial variation of that species.

Semistrong pulse interactions play central roles in a series of pattern formation phenomena, including repelling pulse pairs and self-replication. Repelling pulse pairs in the Gray–Scott model were studied in [3, 4], and this work may be viewed as a continuation of the program

*Received by the editors April 17, 2002; accepted for publication (in revised form) by M. Golubitsky November 5, 2002; published electronically March 31, 2003.
http://www.siam.org/journals/siads/2-1/40571.html
†Korteweg-deVries Instituut, Universiteit van Amsterdam, Plantage Muidergracht 24, 1018TV Amsterdam, The Netherlands (doelman@science.uva.nl). This author was supported by the Organization for Scientific Research (NWO).
‡Department of Mathematics and Center for BioDynamics, Boston University, 111 Cummington Street, Boston, MA 02215 (tasso@math.bu.edu). This author was supported by the National Science Foundation through grant DMS-0072596.

begun there to a broader class of equations. For the Gray–Scott model, ODEs were derived for the time-dependent separation distance between the pulse centers and for their wave speeds. Quantification of the slow spatial variation of the inhibitor concentration in the domain between the pulses was shown to be essential for determining the pulse dynamics.

Self-replication of pulses, discovered and analyzed in the Gray–Scott model [22], is a phenomenon in which a localized pulse splits into two pulses, and as these two pulses move apart from one another, they each split into a pair of pulses so that there are four; see [3, 4, 5, 9, 30, 35, 34, 40, 43, 44]. This process continues, depending on the parameter values and the domain size, until a stationary, spatially periodic pattern is attained. During the entire self-replication process, except near the instants of splitting when the pulse interaction is truly strong, the pulse interactions are semistrong. While the activator concentration is exponentially close to the background state between the pulses due to the singularly perturbed nature of the reaction-diffusion equations, the inhibitor concentration there is not near the value corresponding to the homogeneous steady state and in fact varies on a long spatial-length scale. For instance, in the Gray–Scott model, the pulse interactions are determined largely by the slow spatial variation of the inhibitor concentration on the domain between the pulses, with the local maximum of the inhibitor concentration there increasing slowly in time and in turn causing the pulses to repel each other. We showed in [4] that the time scale of the evolution of this local maximum corresponds to the time scale of pulse-splitting. In addition, recent investigations have shown that self-replication is a rather generic phenomenon that occurs in many reaction-diffusion equations, including the Gierer–Meinhardt equation [21], as has been shown in [10]. Again, the semistrong interaction of pulses plays an essential role.

For a general pair of pulses whose interaction is semistrong, the shapes and amplitudes of the localized pulse-components generally change significantly in time. They are far from being copies of a solitary homoclinic pulse. In fact, there are explicit examples (including the Gray–Scott model and others introduced below) in which pairs of semistrong interacting pulses exist in regions in parameter space where there are no single-pulse homoclinic solutions. In these and other respects, the case of semistrong pulse interaction differs from the weak interaction case (see [12, 14, 42]), where the pulses are to leading order exact, asymptotically stable, single-pulse, homoclinic solutions of the associated reaction-diffusion equation. There, the pulses are assumed to be so far apart that the composition of two pulses is also close to being a solution of the system, and hence the pulses interact through exponentially small tails, they do not change shape to leading order, and they move exponentially slowly away from (or toward) each other in the weak interaction limit. Nevertheless, it is important to note that weak interaction theory applies to a wider range of diffusivities than is considered here; in particular, the diffusivities of both species may be $\mathcal{O}(1)$.

Our study of semistrong pulse interactions is primarily carried out for the following class of coupled reaction-diffusion equations:

$$\begin{cases} \varepsilon^2 U_t &= U_{xx} - \varepsilon^2 \mu U + f(U)V^2, \\ V_t &= \varepsilon^2 V_{xx} - V + g(U)V^2, \end{cases} \tag{1.1}$$

where U and V are positive functions defined for $(x,t) \in \mathbb{R} \times \mathbb{R}^+$, $\mu > 0$ is a parameter, $0 < \varepsilon \ll 1$, and f and g are smooth positive functions on $U > 0$ which may have mild

singularities (poles) at $U = 0$. Many named systems, including the Gierer–Meinhardt, Gray–Scott, Schnakenberg, and Thomas equations (see, for example, [16, 32, 47]) are brought into this specific form (1.1) by scalings that express the asymptotic character of the pulse solutions of singularly perturbed reaction-diffusion equations. See the appendix and Remark 1.1 below. Although ε appears at three places in (1.1), there is, in general, only one small parameter in the original unscaled equation. (ε corresponds to the ratio of the diffusion constants in the Gierer–Meinhardt model, while ε is in essence a certain ratio between constants describing the linear feed terms in the Gray–Scott model; see the appendix and [3, 4, 7].)

The choice of a relatively general system (1.1) was motivated by the following types of questions. In the Gray–Scott model [3, 4] and in the Gierer–Meinhardt equation (section 5), the pulses in a two-pulse solution repel. What mechanism(s) causes the pulses to repel, and is it possible to find systems for which pulses attract? Next, two repelling pulses might eventually be so far apart that their interaction can be studied by the theory of weak interactions. So, we ask, Will a pair of pulses necessarily enter the domain in which the interactions can be considered as weak? We will see in sections 5 and 6 that this is not the case and that several interesting things may happen depending on parameters and the nonlinearities. In addition, we focus on the edge of the parameter domains in which two-pulse solutions exist. A hierarchy of saddle-node points at which stable N-pulse solutions, $N = 1, 2, \ldots$, disappear has been found for the Gray–Scott and Gierer–Meinhardt equations, and this hierarchy governs the self-replication process; see [3, 4, 5, 10, 34, 35]. Are there new phenomena, in addition to self-replication, that occur at the edge of the parameter domains in which the pulse solutions exist? Here, we will see that the answer is yes, and we will determine their relation to self-replication. Finally, we have formally determined the stability of two-pulse solutions for the Gray–Scott model in [3]. Hence we also briefly ask about the stability of the pulse solutions for the general class of systems and about the related issue of the validity of the asymptotic constructions.

Based on the analysis presented in this article, we find that the essential properties of the reaction terms in (1.1) are

(i) the number and location of the zeros of $g'(U)$ and the sign of $g'(U)$ for values of U that are not zeros; and

(ii) the number and location of the zeros of the function $H(U) \equiv (3f(U)/g^2(U)) - \sqrt{\mu}U$.

Properties (i) and (ii), which emerge naturally from the system geometry, determine the salient features of the pulse dynamics. First, the number of zeros of H in (ii) is the number of different stationary, homoclinic, one-pulse solutions the equation has. Second, the zeros of H also determine the allowable locations (in the $U - V$ plane) of the pulses in multipulse solutions. Specifically, each zero corresponds to an allowable pair of jump off and jump on points, which mark the left and right "edges" of the pulses, on a certain invariant manifold. Third, the information in property (i) determines whether adjacent pulses attract or repel each other, as well as whether asymmetric two- and N-pulse solutions can be constructed in addition to symmetric ones.

Our first set of results concerns slowly varying two-pulse solutions, i.e., two-pulse solutions in which the pulse centers move with slowly varying speeds $c_1(t)$ and $c_2(t)$ and the pulse shapes (amplitudes and widths) vary slowly in time for systems of the form (1.1), in which (i) $g'(U)$ has no zeros on $U > 0$ and (ii) the function $H(U) = (3f(U)/g^2(U)) - \sqrt{\mu}U$ has one positive

simple zero. We derive the ODE for the pulse separation distance, denoted $\Delta\Gamma(t)$, as well as the extremal values of the pulse speeds. We find that $\Delta\Gamma(t)$ decreases (and the pulses attract) for configurations in which $g'(U) > 0$, whereas $\Delta\Gamma(t)$ increases (and the pulses repel each other) in those cases for which $g'(U) < 0$. The different signs of $g'(U)$ also appear to be directly connected to the stability of these solutions.

The second set of results concerns system (1.1) for which (i) $g'(U)$ has one positive simple zero and (ii) the function $H(U)$ again has one positive simple zero. For these systems, both stationary and slowly varying two-pulse solutions can exist. Moreover, for the slowly varying solutions, the pulses can either attract or repel each other, and the rates of approach or repulsion can be increasing or decreasing or can even change dynamically in time from being increasing to decreasing or vice versa. The particulars of whether a stationary two-pulse solution exists or of what dynamics a slowly varying two-pulse solution exhibits are determined by where the zero of $g'(U)$ lies with respect to the U value that corresponds to the maximum of a stationary one-pulse solution and to the local maximum of U for the pulse solutions with extremal speed. Here, we see that a pair of repelling pulses may limit, in time, on a stationary two-pulse solution. Such a pair, therefore, will not reach the weak interaction limit.

We also present extensions of the above two principal sets of results. The first extension is to a more general class of systems,

$$\left\{ \begin{array}{rcl} \varepsilon^{2+\sigma} U_t &=& U_{xx} + \varepsilon^2 F_1(U) + V F_2(U,V), \\ V_t &=& \varepsilon^2 V_{xx} + G(U,V). \end{array} \right. \tag{1.2}$$

Here, $\sigma \geq 0$, $0 < \varepsilon \ll 1$, and the functions F_1, F_2, and G are smooth for $U > 0$ and $V \geq 0$ and admit at most poles at $U = 0$. They must also satisfy additional assumptions, which we state in section 7.

The second extension is to N-pulse solutions of (1.1) for $N \geq 2$, including stationary solutions, classical traveling wave solutions, in which the entire N-pulse solutions moves with constant wave speed, and slowly varying solutions. The slowly varying N-pulse solutions are useful for understanding more about self-replication. At the stage of self-replication in which the data has N pulses, one can use the ODEs for the positions of the N-pulse centers and knowledge of the parameter regimes in which they exist and are stable to determine if the pulses (some or all) will split again or if instead the self-replication process ends and the asymptotic state is an N-pulse solution.

The classical Gierer–Meinhardt model is of the form (1.1) with $f(U) \equiv 1$ and $g(U) = 1/U$, and the generalized Gierer–Meinhardt model [7, 33] is of the form (1.2). The ODEs we derive for the pulse separation distances and for the pulse speeds show that the pulses of a slowly varying two-pulse solution repel each other; see also Figure 1.1. Moreover, these results can be used to further understand the self-replication recently discovered [10] in the Gierer–Meinhardt model in the same way as the ODEs for the pulse separation distances were used for the Gray–Scott model in [4].

In addition to obtaining the above results, we have the overarching goal of determining the boundaries of the existence domains in parameter space for the various two-pulse solutions and N-pulse solutions in the semistrong interaction regime. These boundaries have already been shown to be important for self-replication (see the discussion below). Here, we show that

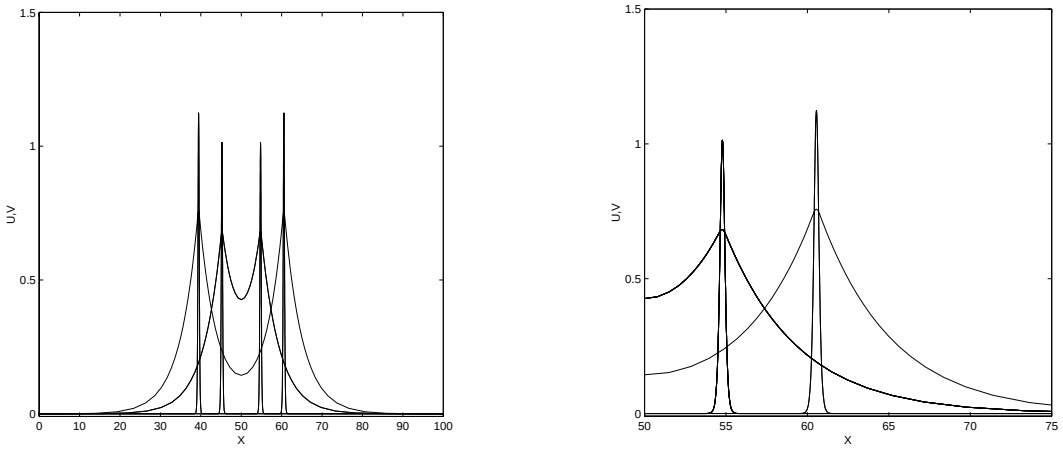

Figure 1.1. *A symmetric, slowly varying, two-pulse solution obtained from direct numerical simulations of the classical Gierer–Meinhardt equation for* $\varepsilon^2 = 0.01$ *and* $\mu = 5$ *shown at two instants of time. The pulses repel each other, as is shown in section 5, and the ODE (5.6) governs the time-dependent separation distance between the pulses. In the left frame, the slowly varying two-pulse solution is shown at two instants of time; in the first instant, the two pulses are the inner pair with smaller maxima, while in the second instant, the pulses are further separated and have larger maxima. The right frame is a magnification of part of the right half of the domain in the left frame, shown so that the pulse structure is more clearly visible. The* V *(activator) component has the narrow needle-like pulses and is vanishingly small on the intervals in between the pulses, while the* U *(inhibitor) component has pulses with lower maxima and varies over a much longer length scale. The inhibitor concentration* U *in between the two pulses is not near zero, the value of the homogeneous steady state, and its local minimum in between the pulses slowly decreases. The numerically observed values of the maxima of* U *and* V *at the pulse peaks agree well with the theory presented here. Homogeneous Neumann boundary conditions and* $N = 201$ *moving grid points were used on the scaled interval* $[0, 1]$*. This and all other numerical simulations in this article have been performed using the code presented in* [2].

the boundaries of the existence domains can also correspond to bifurcation curves associated to the blowup in finite time of localized pulse solutions. On one side of these curves, blowup is observed, but none is observed on the other side. Moreover, we have found an example in which there is a self-replication bifurcation curve that meets a blowup bifurcation curve in a new type of codimension two point, which we label a self-replication/blowup bifurcation point.

The blowup phenomenon was discovered in two examples introduced here to illustrate the theory of semistrong pulse interaction. The first example is (1.1) with $f(U) \equiv 1$ and $g(U) = (1/U)+\alpha$, and the second example is (1.1) with $f(U) \equiv 1$ and $g(U) = (1/U)+(\beta/\sqrt{U})$. The classical Gierer–Meinhardt equation is a special case of both examples, with $\alpha = 0$ and $\beta = 0$, respectively, although the blowup we find in both problems occurs for nonzero values of these parameters.

For the first example, slowly varying two-pulse solutions can exist in parameter regimes in which there is no stationary, homoclinic, one-pulse solution. Since $g'(U) < 0$ for all $U > 0$ and for all $\alpha \geq 0$, the pulses in a slowly varying two-pulse solution repel each other. As a consequence, (to leading order) both pulses necessarily evolve toward a copy of the nonexisting stationary one-pulse solution. It follows from the theory developed in this article that there

is a critical separation distance, $\Delta\Gamma_{bu}$, beyond which the two-pulse solution can no longer be constructed. Numerical simulations show that at $t = t_{bu}$, the time when a solution reaches the critical separation distance, which of course depends on initial conditions, one of the pulses starts to grow extremely rapidly, without bound.

In the second modified Gierer–Meinhardt example, the two interacting pulses can also exist in parameter regimes in which there is no stationary, homoclinic, one-pulse solution, and they also repel (again $g'(U) < 0$ for all $U > 0$ and for all $\beta \geq 0$). Most significantly, they can develop asymptotically large amplitudes as a result of the semistrong interaction. This finite-time blowup can be understood in full analytical detail, with explicit formulae for how both components grow and for the time of the blowup. It differs in some important respects from that observed in the first example.

There are many important characteristics of the Gray–Scott and Gierer–Meinhardt equations (see [4, 10]) that are shared by the two new examples introduced here. As just stated, one of the more interesting of these characteristics is that the slowly varying two-pulse solutions not only exist in the parameter regions where the stationary, homoclinic, one-pulse solutions exist, but they can also exist outside of those regions. Then, for parameter values outside of those regions, the individual pulses of a two-pulse solution tend to copies of the one-pulse, leaving one with the question of what should happen to them since the one-pulse solutions do not exist there. This question was addressed in the context of the self-replication process in the Gray–Scott model in [4] by introducing the notion of an effective small parameter whose size depends on the slowly changing magnitude of the U- (inhibitor) component at the local maximum in between the pulses. For two-pulse solutions in which the pulses are still close together, that magnitude is sufficiently small, and the effective small parameter is such that one is still back in the regime where the one-pulse exists (and is stable; see [5, 6]). However, as that magnitude increases slowly in time, the effective small parameter eventually crosses the self-replication threshold so that the pulses, which could not continue to exist as copies of the nonexistent one-pulse solutions, split just as the initial one-pulse data did. Correspondingly, there is a hierarchy of disappearance (or saddle-node) bifurcations that governs the boundary of the self-replication domain in parameter space, as reported in [5, 4, 34, 35], and a similar analysis can be carried out for splitting in the Gierer–Meinhardt model; see [10].

The analysis presented here shows that this same question arises for the two modified Gierer–Meinhardt examples and has a similar type of answer; only here, the slowly varying two-pulse solutions and the stationary, homoclinic, one-pulse solutions can exhibit finite-time blowup, as well as splitting, depending on parameters.

This article is organized as follows. Section 2 contains the essential geometric information about the invariant manifolds. The basic construction of slowly varying two-pulse solutions is presented in section 3. Section 4 contains the study of symmetric, slowly varying, two-pulse solutions and the presentation of the first set of results. Three examples, including the two that exhibit finite-time blowup, are introduced and analyzed in section 5. Section 6 contains the second set of main results for stationary and slowly varying two-pulse solutions in systems that support more than a single stationary, homoclinic, one-pulse solution. Finally, in section 7, we discuss the extensions of the above results, including extensions to N-pulse solutions and generalizations to the broader class of coupled reaction-diffusion equations given by (1.2). We also discuss the stability of the solutions constructed here and the validity of the asymptotic

constructions.

Remark 1.1. For the PDEs (1.1) and (1.2), one may assume without loss of generality that the state $(U_0, V_0) = (0, 0)$ is a homogeneous steady state. Moreover, we assume that $(0, 0)$ is a linearly stable solution of the PDEs with $\mu > 0$. As shown in the appendix, this may entail a change of dependent variables such as is the case, for example, in the Gray–Scott model, which has $(1, 0)$ as a linearly stable homogeneous state. It may also entail ensuring that the solution components vanish at certain rates (see [7]), as is necessary for the generalized Gierer–Meinhardt equations, where $g(U) = 1/U$ as stated above, so that one needs V^2 to vanish more rapidly than U along solutions in order for the quotient to vanish.

Remark 1.2. Pulse interactions have also been analyzed in other contexts, and we mention some recent references without being exhaustive. In [38], one-dimensional (particle-like) pulses in the excitable regime of a coupled reaction-diffusion system of FitzHugh–Nagumo type are studied. The dispersion relation $c(d)$ for the speed of pulse-trains as a function of their wavelengths is presented, and a transition from long range dispersion (common in excitable systems) to anomalous dispersion, for large d, is found that is shown to be responsible for a long range attractive force between pulses. They also demonstrate the existence of stable bound states. [36] examines the dynamics of sharp interfaces in an activator-inhibitor model with global coupling in one and two spatial dimensions. It is shown that a pair of fronts that initially approach can reflect off of one another and then repel each other. Next, [13] reports on the discovery of pulse reflection in a two-component excitable system. Moreover, it is shown that reflections also occur for spirals and rings in two space dimensions, and the bifurcations are analyzed using center manifold theory for sufficiently small pulse velocities. Finally, two-dimensional pulses are also analyzed in an activator-inhibitor system with global coupling in [26]. The bifurcation of a stationary pulse to a traveling pulse is examined using interface dynamics, and the collision of two pulses is also observed in the presence of sufficiently strong global coupling.

2. Geometry of the invariant manifolds. In this section, we present the phase space geometry associated to the pulse solutions studied in this article. Let $c(t)$ denote the time-dependent velocity of a pulse, and let $x = \Gamma(t)$ denote the time-dependent position of the pulse's center, where

$$\Gamma(t) = \int_{t_0}^{t} c(s)ds. \tag{2.1}$$

It is also useful to introduce the moving coordinate, $\bar{x} = x - \Gamma(t)$, as well as a stretched moving coordinate, $\xi \equiv \bar{x}/\varepsilon$.

Looking ahead just a bit, we can also take advantage of the following two observations. First, the distinguished wave speed is small,

$$c(t) \equiv \varepsilon^3 \hat{c}(t), \tag{2.2}$$

where $\hat{c}(t)$ is $\mathcal{O}(1)$, and $|d\hat{c}/dt| \ll 1$. This agrees with the earlier analysis [3, 4] of self-replication and semistrong pulse interactions in the Gray–Scott model and will be shown to be a distinguished speed also for the general systems (1.1). See Remark 2.2 below. Second, it turns out that, for the solutions we study, the explicit time variation of U and V is also slow, i.e., $|\partial U/\partial t|, |\partial V/\partial t| \ll 1$. Therefore, we use a quasi-stationary approximation, which

entails treating $\hat{c}(t)$ as a slowly varying parameter that lies within a certain allowable range and ignoring the explicit partial derivatives with respect to t to leading order. Hence, to leading order, the solutions $(U(\xi(t),t),V(\xi(t),t))$ depend only on t through $\xi(t)$. (See also Remark 3.1 for a brief discussion of higher order terms and the validity of this quasi-stationary approximation.)

Within the context of this quasi-stationary approximation, the quasi-stationary solutions of the PDE (1.1) are described by the following system of four first order ODEs:

$$\left\{\begin{array}{rcl} \dot{u} &=& \varepsilon p, \\ \dot{p} &=& \varepsilon\left[-\varepsilon^5\hat{c}p+\varepsilon^2\mu u - f(u)v^2\right], \\ \dot{v} &=& q, \\ \dot{q} &=& -\varepsilon^2\hat{c}q+v-g(u)v^2. \end{array}\right. \tag{2.3}$$

Here, $u(\xi)$ and $v(\xi)$ are the leading order terms in the asymptotic expansions of the solutions $(U(\xi(t),t),V(\xi(t),t))$ of the PDE (1.1), and the overdot denotes derivatives with respect to ξ. Also, $\hat{c}=\hat{c}(t)$ is a parameter.

2.1. A normally hyperbolic invariant manifold for (2.3). One natural approach to determining the relevant geometrical features of the phase space of the ODE (2.3) is to identify the structures that exist when $\varepsilon=0$ and then to ask which of these persist for $0<\varepsilon\ll 1$.

For $\varepsilon=0$, the half-plane

$$\mathcal{M}=\{(u,p,v,q)|v=0,q=0,u>0\} \tag{2.4}$$

is a set of equilibrium points of (2.3). Off of $\mathcal{M}$, the system exhibits fast dynamics governed by the fast system

$$\left\{\begin{array}{rcl} \dot{v} &=& q, \\ \dot{q} &=& v-g(u)v^2, \end{array}\right. \tag{2.5}$$

where u is a fixed parameter. This fast system has the conserved quantity (energy)

$$K(v,q;u)=\frac{q^2}{2}-\frac{v^2}{2}+\frac{g(u)}{3}v^3. \tag{2.6}$$

Moreover, each fixed point $(u,p,0,0)$ on $\mathcal{M}$ is a saddle point under the flow (2.5). Hence the two-dimensional invariant plane $\mathcal{M}$ is normally hyperbolic. Finally, since $g(u)>0$ for $u>0$, each fixed point on $\mathcal{M}$ is connected to itself by a homoclinic orbit $(v_0(\xi),q_0(\xi))$, where

$$v_0(\xi)=\frac{3}{2g(u)}\mathrm{sech}^2\left(\frac{\xi}{2}\right), \tag{2.7}$$

of the fast system (2.5). Therefore, the three-dimensional stable and unstable manifolds of $\mathcal{M}$, denoted $W^S(\mathcal{M})$ and $W^U(\mathcal{M})$, coincide.

For $0<\varepsilon\ll 1$, the plane $\mathcal{M}$ is still an invariant set under the dynamics of (2.3), and it still has three-dimensional stable and unstable manifolds by the Fenichel theory of geometric singular perturbations; see [18] and [24]. On $\mathcal{M}$, the system (2.3) reduces to

$$\left\{\begin{array}{rcl} \dot{u} &=& \varepsilon p, \\ \dot{p} &=& \varepsilon^3(\mu u-\varepsilon^3\hat{c}p). \end{array}\right. \tag{2.8}$$

The equilibrium point S, $(u,p)=(0,0)$, of (2.8) on the boundary of $\mathcal{M}$ corresponds to the homogeneous state $(U_0,V_0)=(0,0)$ of (1.1), and it is a saddle equilibrium in the phase space of (2.8). Moreover, the stable and unstable manifolds of S restricted to $\mathcal{M}$, labeled ℓ^s and ℓ^u, are given to leading order by the lines

$$\ell^s,\ell^u: \qquad p=\mp\varepsilon\sqrt{\mu}u. \tag{2.9}$$

We are interested in that portion of $\mathcal{M}$ that lies in the wedge between (or on) ℓ^u and ℓ^s. In this wedge, the p-coordinates of all points are at most $\mathcal{O}(\varepsilon)$, and so it is useful to explicitly introduce $p=\varepsilon\hat{p}$, where $\hat{p}=\mathcal{O}(1)$.

Remark 2.1. For general $g(u)$, the boundary $u=0$ is excluded from the definition of $\mathcal{M}$, since $g(u)$ may have a pole there. In that case, one can still obtain results for those solutions along which v vanishes sufficiently rapidly so that the product $g(u)v^2$ vanishes. The method employed in [7] (see the end of section 2.4 there) to analyze semistrong pulses in the generalized Gierer–Meinhardt equation extends to system (1.1). Of course, if g is also smooth at $u=0$, such as in the Gray–Scott model (transformed as in the appendix), then one can include the boundary as part of the manifold.

2.2. Persistent orbits homoclinic to $\mathcal{M}$. For $0<\varepsilon\ll 1$, the stable and unstable manifolds of $\mathcal{M}$ no longer coincide. Instead, they are expected to intersect transversely in a two-dimensional surface, in which all orbits that are biasymptotic ($\xi\to\pm\infty$) to $\mathcal{M}$ lie. We find this surface in this section.

For points on $\mathcal{M}$, $K=0$. Hence orbits that are biasymptotic to $\mathcal{M}$ satisfy

$$\Delta K\equiv\int_{-\infty}^{\infty}\dot{K}(v(\xi),q(\xi);u(\xi))d\xi=0 \tag{2.10}$$

so that their α and ω limit sets are both on $\mathcal{M}$. By adiabatic Melnikov function theory [45], simple zeros of ΔK imply the existence of nearby transverse intersections of the manifolds $W^S(\mathcal{M})$ and $W^U(\mathcal{M})$.

Let $(u(\xi),p(\xi),v(\xi),q(\xi))$ denote any solution of (2.3) that, at $\xi=0$, passes through the hyperplane $\{q\equiv 0\}$ with $u,v>0$ and with p in the desired wedge. Denote such a point on $\{q\equiv 0\}$ by $(u,\varepsilon\hat{p},v(0),0)$. A straightforward calculation of $\dot{K}$ along these solutions of (2.3) yields

$$\dot{K}=\varepsilon^2\left(-\hat{c}q^2+\frac{\hat{p}}{3}g'(u)v^3\right). \tag{2.11}$$

Thus a solution $(u(\xi),p(\xi),v(\xi),q(\xi))$ of the type under consideration here is a persistent homoclinic orbit to $\mathcal{M}$ if

$$\varepsilon^2\int_{-\infty}^{\infty}\left(-\hat{c}q^2(\xi)+\frac{\hat{p}(\xi)}{3}g'(u(\xi))v^3(\xi)\right)d\xi=0. \tag{2.12}$$

For $0<\varepsilon\ll 1$, the persistent homoclinic orbits in the transverse intersection of $W^U(\mathcal{M})$ and $W^S(\mathcal{M})$ lie close to their $\varepsilon=0$ counterparts. Specifically, persistence theory for invariant manifolds [18] establishes that solutions on $W^U(\mathcal{M})$ and $W^S(\mathcal{M})$ are close to the unperturbed homoclinic orbit $(v_0(\xi),q_0(\xi)=\dot{v}_0(\xi),u,0)$ on appropriate time intervals, $(-\Xi,\xi_0)$ and (ξ_0,Ξ),

respectively, where Ξ may be taken arbitrarily large (but $\mathcal{O}(1)$) as long as ε is sufficiently small.

Therefore, asymptotically, we may approximate $u(\xi)$ by the constant u, $v(\xi)$ by $v_0(\xi)$ as given by (2.7), and $q(\xi)$ by $q_0(\xi)$. Hence, to leading order, condition (2.12) implies that either $\hat{c} = 0$ (which is the case when $g'(u) = 0$) or

$$\hat{p} = 2\hat{c}\frac{g(u)}{g'(u)} \tag{2.13}$$

(which is the case when $g'(u) \neq 0$ for all $u > 0$). Here, we used the intermediate results $\int_{-\infty}^{\infty} q_0^2 d\xi = 6/(5g^2(u))$ and $\int_{-\infty}^{\infty} v_0^3 d\xi = 36/(5g^3(u))$.

Geometrically, this result may be understood as follows. In the first case, there is a one-parameter family of orbits biasymptotic to $\mathcal{M}$, and these have the symmetry $(u, p, v, q) \to (u, -p, v, -q)$ about $\xi = 0$. In the second case, there is also a one-parameter family of orbits biasymptotic to $\mathcal{M}$. However, they are not symmetric. Instead, those orbits $(u(\xi), p(\xi), v(\xi), q(\xi))$ with $(u, \varepsilon\hat{p}, v(0), 0)$ at $\xi = 0$ and $v(0)$ near $v_0(0) = 3/(2g(u))$ that are biasymptotic to $\mathcal{M}$ satisfy the property that their u- and p-coordinates are related by (2.13) to leading order. Therefore, since $g(u) > 0$ by assumption, the sign of $\hat{p}$ is determined by the signs of $\hat{c}$ and $g'(u)$. This property will be essential throughout the analysis.

Finally, during the "time" interval when the homoclinic orbits in the transverse intersection of $W^U(\mathcal{M})$ and $W^S(\mathcal{M})$ make their excursion through the fast field, i.e., when they lie outside of a fixed neighborhood of $\mathcal{M}$, their slow coordinates u and p undergo changes that are given to leading order by

$$\Delta u \equiv \int_{-\infty}^{\infty} \dot{u}(\xi) d\xi \qquad \text{and} \qquad \Delta p \equiv \int_{-\infty}^{\infty} \dot{p}(\xi) d\xi. \tag{2.14}$$

Now, since $p = \varepsilon\hat{p}$ and $\hat{p} = \mathcal{O}(1)$ for these orbits, we immediately see from (2.3) that

$$\Delta u = \mathcal{O}(\varepsilon^2). \tag{2.15}$$

Hence u is actually constant to a higher degree of approximation than originally stated. Moreover, with $u \sim$ constant, we find

$$\begin{aligned} \Delta p(u, \hat{c}) &= -\varepsilon \int_{-\infty}^{\infty} f(u) v^2 d\xi + \text{h.o.t.} \\ &= -\varepsilon f(u) \int_{-\infty}^{\infty} v_0^2 d\xi + \text{h.o.t.} \\ &= -6\varepsilon \frac{f(u)}{g^2(u)} + \text{h.o.t.} \end{aligned} \tag{2.16}$$

This change in p during the fast jump plays a central role in much of the geometry of the pulses and hence also in much of the analysis in this article.

Remark 2.2. That $c(t) = \varepsilon^3 \hat{c}(t)$ is a distinguished wave speed as introduced in (2.2) above can be seen directly from the adiabatic Melnikov condition (2.12). One wants to balance the first and second terms in order that ΔK can have zeros. The second term is $\mathcal{O}(\varepsilon^2)$, and hence

if one scales $c = \mathcal{O}(\varepsilon^3)$, then also the first term is $\mathcal{O}(\varepsilon^2)$. This is a distinguished limit; see [11].

Remark 2.3. In the special case in which $g(u) = h_2 u^{\alpha_2}$ with $h_2 > 0$ and $\alpha_2 < 0$, such as, for example, in the Gierer–Meinhardt equation and in its generalizations, we have $g(u)/g'(u) = u/\alpha_2$. Hence $\hat{p} = \hat{p}(u) = (2\hat{c}/\alpha_2)u$, a linear function.

Remark 2.4. We have focused exclusively on the geometry used to construct one-pulse solutions in this section. Multiple-pulse solutions that consist of two slow segments and one fast segment in which all of the pulses occur in rapid succession (i.e., they remain bounded away from $\mathcal{M}$ in between pulses) can also be constructed, but such stationary solutions are unstable solutions of the PDE; see [7].

2.3. The takeoff and touchdown curves for persistent homoclinic orbits. There are takeoff and touchdown curves on $\mathcal{M}$ that play a crucial role in the geometry of the pulse solutions. These are determined by the two-dimensional manifold that is the transverse intersection of $W^U(\mathcal{M})$ and $W^S(\mathcal{M})$ identified in the previous section. The first intersection of $W^S(\mathcal{M})$ and $W^U(\mathcal{M})$ in the hyperplane $\{q = 0\}$ is a one-dimensional curve of points $(u, \varepsilon\hat{p}, v(0), 0)$, where u and $\hat{p}$ are related to leading order via (2.13) in this two-dimensional manifold. Moreover, through any such point there is an orbit $\gamma(\xi;\gamma_0)$ with phase γ_0 that approaches $\mathcal{M}$ as $\xi \to \pm\infty$. Fenichel theory [18] implies that for any $\gamma(\xi;\gamma_0)$ there are two orbits $\gamma^+_{\mathcal{M}} = \gamma^+_{\mathcal{M}}(\xi;\gamma_0^+) \subset \mathcal{M}$ and $\gamma^-_{\mathcal{M}}(\xi;\gamma_0^-) \subset \mathcal{M}$, respectively (where $\gamma^\pm_{\mathcal{M}}(0,\gamma_0^\pm) = \gamma_0^\pm \in \mathcal{M}$), such that $\|\gamma(\xi;\gamma_0) - \gamma^+_{\mathcal{M}}(\xi;\gamma_0^+)\|$ is exponentially small for positive values of ξ that satisfy $\xi \geq \mathcal{O}(\frac{1}{\varepsilon})$ and $\|\gamma(\xi;\gamma_0) - \gamma^-_{\mathcal{M}}(\xi;\gamma_0^-)\|$ is exponentially small for $\xi < 0$ satisfying $-\xi \geq \mathcal{O}(\frac{1}{\varepsilon})$. As a consequence,

$$d(\gamma(\xi;\gamma_0),\mathcal{M}) = \mathcal{O}\left(e^{-\frac{k}{\varepsilon}}\right) \quad \text{for} \quad |\xi| \geq \mathcal{O}\left(\frac{1}{\varepsilon}\right) \quad \text{and some } k > 0,$$

and the orbits $\gamma^\pm_{\mathcal{M}}(\xi;\gamma_0^\pm)$ on $\mathcal{M}$ determine the behavior of $\gamma(\xi;\gamma_0)$ near $\mathcal{M}$.

We define the curves $T_o(\hat{c}) \subset \mathcal{M}$ (takeoff) and $T_d(\hat{c}) \subset \mathcal{M}$ (touchdown) as

$$\begin{aligned} T_o(\hat{c}) &= \cup_{\gamma_0}\{\gamma_0^- = \gamma^-_{\mathcal{M}}(0;\gamma_0^-)\}, \\ T_d(\hat{c}) &= \cup_{\gamma_0}\{\gamma_0^+ = \gamma^+_{\mathcal{M}}(0;\gamma_0^+)\}, \end{aligned} \tag{2.17}$$

where the unions are over all γ_0 in $W^S(\mathcal{M}) \cap W^U(\mathcal{M}) \cap \{q = 0\}$. Therefore, the curves $T_o(\hat{c})$ and $T_d(\hat{c})$ are the collections of the basepoints of all of the fibers in $W^U(\mathcal{M})$ and $W^S(\mathcal{M})$ (respectively) that lie in the transverse intersection of these two manifolds. See Figure 2.1.

Asymptotic formulas for the locations of $T_o(\hat{c})$ and $T_d(\hat{c})$ can be obtained as follows. The accumulated changes in the p-component of $\gamma(\xi)$ during two successive half-circuit excursions through the fast field are measured by

$$\int_{-\infty}^{0} \dot{p}d\xi \qquad \text{and} \qquad \int_{0}^{\infty} \dot{p}d\xi,$$

respectively, and these integrals may be calculated by the same method used to obtain (2.16). Moreover, at $\xi = 0$, the orbits have $\hat{p}$ given by (2.13). Hence we find

$$T_o(\hat{c}), T_d(\hat{c}): \qquad \hat{p} = 2\hat{c}\frac{g(u)}{g'(u)} \pm \frac{3f(u)}{g^2(u)}. \tag{2.18}$$

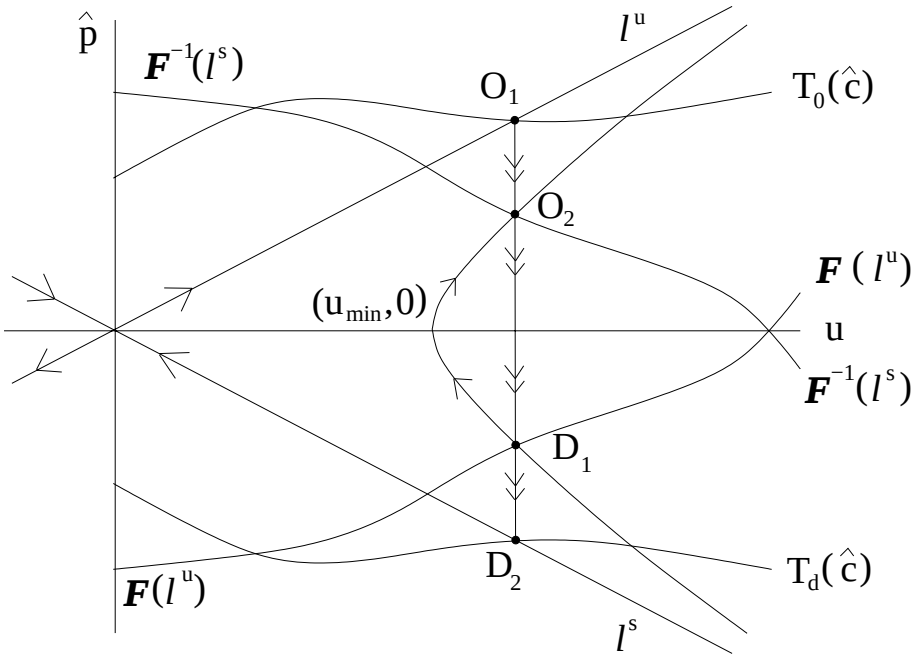

Figure 2.1. *A qualitative sketch of the curves $T_o(\hat{c})$, $T_d(\hat{c})$, $\mathcal{F}(\ell^u)$, and $\mathcal{F}^{-1}(\ell^s)$ on $\mathcal{M}$, as defined in section 2, as well as of a singular, slowly varying, two-pulse solution, whose construction is outlined in section 3. The sketch is for the symmetric case $\hat{c}_2 = -\hat{c}_1$. The successive slow, fast, and slow segments of the left pulse are from $(0,0)$ to O_1, O_1 to D_1, and D_1 to $(u_{\min},0)$, respectively. We remark that the line segments $\overline{O_1D_1}$ and $\overline{O_2D_2}$ are projections onto $\mathcal{M}$ of the fast near-homoclinic excursions in the $v-v_\xi$ directions. Also, we emphasize that $T_o(\hat{c})$ is a one-dimensional curve for each fixed value of $\hat{c}=\hat{c}_1$, and similarly for $T_d(\hat{c})$. By contrast, $\mathcal{F}(\ell^u)$ is a one-dimensional curve because it is the union over a certain range of $\hat{c}$ values of touchdown points—one for each value of $\hat{c}$. Similarly, $\mathcal{F}^{-1}(\ell^s)$ is a one-dimensional curve because it is the union of takeoff points—again one point for each $\hat{c}$ in a certain range. See the definitions in section 2.4.*

2.4. The images of the intersection points $\ell^u \cap T_o(\hat{c})$ and $\ell^s \cap T_d(\hat{c})$ under the fast jump. As a final preparatory step, we identify two other curves on $\mathcal{M}$ that will be useful throughout the analysis. In particular, for those values of $\hat{c}$ for which the intersections $\ell^u \cap T_o(\hat{c})$ and $\ell^s \cap T_d(\hat{c})$ exist, we are interested in the image of $\ell^u \cap T_o(\hat{c})$ and in the preimage of $\ell^s \cap T_d(\hat{c})$.

We showed in section 2.2 that, for fixed $\hat{c}$, a persistent homoclinic orbit to $\mathcal{M}$ that takes off from a point on $T_o(\hat{c})$ touches down on $\mathcal{M}$ at a point that has the same u-coordinate to leading order and whose p-coordinate is shifted by $\Delta p(u,\hat{c})$. This same conclusion holds, of course, for points that take off at the intersection point $\ell^u \cap T_o(\hat{c})$, if this intersection exists. The union over $\hat{c}$ of all of these touchdown points is denoted by $\mathcal{F}(\ell^u)$. See Figure 2.1. To leading order, $\mathcal{F}(\ell^u)$ is given by

$$\mathcal{F}(\ell^u): \qquad \hat{p} = \sqrt{\mu}u - \frac{6f(u)}{g^2(u)}. \tag{2.19}$$

Similarly, let $\mathcal{F}^{-1}(\ell^s)$ denote the set of points that are the preimages (takeoff points) under the fast jump of the touchdown points in $\ell^s \cap T_d(\hat{c})$ over all $\hat{c}$, when this intersection exists.

To leading order,

$$\mathcal{F}^{-1}(\ell^s): \quad \hat{p} = -\sqrt{\mu}u + \frac{6f(u)}{g^2(u)}. \tag{2.20}$$

These curves play a central role in the definition of the function H introduced above.

3. The basic construction of slowly varying two-pulse solutions. In this section, we present a brief introduction to slowly varying two-pulse solutions, focusing on the basic idea of how the geometry of the invariant manifolds described in the previous section is used to construct them. Specifically, we consider slowly varying two-pulse solutions with one pulse on $x \le x_0$ for some $x_0 \in \mathbb{R}$ that travels with speed $c_1(t)$ and the other on $x \ge x_0$ that travels with speed $c_2(t)$.

The moving coordinate $\bar{x} = x - \Gamma_1(t)$, with $\Gamma_1(t) = \int_{t_0}^{t} c_1(s)ds$, is used to analyze the left pulse, and hence the governing ODE is (2.3) with $\hat{c} = \hat{c}_1$ slowly changing in time. The results for the right pulse are obtained from the same ODE but with $\hat{c} = \hat{c}_2$ instead changing slowly in time, and the geometry for it is usually shown superimposed in the same phase space as for the left pulse. We refer the reader to Remark 3.1 and section 7 for a discussion of how these two components are hooked up smoothly and of the justification of this asymptotic construction.

The $\hat{c}_1$ values for which the two-pulse solutions can be constructed depend on the quantities in (i) and (ii), as we show in the next sections.

3.1. Constructing singular two-pulse solutions. The left pulse, centered at $x = \Gamma_1(t)$, is asymptotic to $(U, V) = (0, 0)$ as $x \to -\infty$ and satisfies a Neumann boundary condition $(U_x, V_x = 0)$ at $x = x_0$. In fact, the singular ($\varepsilon \to 0$) limit of the left pulse consists of the following three pieces (see Figure 2.1), two slow (outer) segments on $\mathcal{M}$ interspersed with a fast (inner) homoclinic orbit of the reduced fast system (2.5):

- The left slow segment corresponds to the interval $(-\infty, \Gamma_1(t))$ and is that portion of ℓ^u on $\mathcal{M}$ from $(0, 0)$ to the point, labeled O_1, at which $T_o(\hat{c}_1)$ and ℓ^u intersect transversely.
- The fast pulse is centered at $x = \Gamma_1(t)$ and is described in the stretched coordinate ξ introduced above. To leading order, it is given by $(v_0(\xi), q_0(\xi))$, see (2.7), with u constant. Over the fast pulse, the p-component makes a jump $\Delta p(u; \hat{c})$ of size $\mathcal{O}(\varepsilon)$ (see (2.16)). Therefore, the projection of this fast jump onto the $u-p$ plane is precisely the vertical line segment from O_1 to the point labeled D_1 on $\mathcal{F}(\ell^u)$.
- The right slow segment, which corresponds to $x \in (\Gamma_1(t), x_0]$, is that segment of the hyperbolic cosine orbit on $\mathcal{M}$ from D_1 to a point on $p = 0$ labeled $(u_{\min}, p = 0)$, so that the homogeneous Neumann boundary condition is satisfied.

The singular right pulse is now constructed in a similar manner on $x > x_0$. It has a left slow segment, which corresponds to $x \in [x_0, \Gamma_2(t))$, that is the continuation of the hyperbolic cosine solution on $\mathcal{M}$ (but for the ODE with $\hat{c} = \hat{c}_2$ now) from $(u_{\min}, 0)$ to a point on $\mathcal{F}^{-1}(\ell^s)$ labeled O_2. Note that the difference between $\hat{c} = \hat{c}_1$ and $\hat{c} = \hat{c}_2$ is a higher order effect in (2.3); see also Remark 3.1. The projection of the fast homoclinic orbit on $\mathcal{M}$ is the vertical line segment from O_2 to D_2, where $D_2 \in T_d(\hat{c}_2) \cap \ell^s$. Finally, the right slow segment, which corresponds to $x \in (\Gamma_2(t), \infty)$, is that portion of ℓ^s from D_2 to S; see Figure 2.1.

3.2. Slowly varying two-pulse solutions for $0 < \varepsilon \ll 1$ lie close to the singular two-pulse solutions. For $0 < \varepsilon \ll 1$ and $x < \Gamma_1(t) - \delta$ with $\delta > 0$ small but $\mathcal{O}(1)$, the left pulse lies exponentially close to ℓ^u on $\mathcal{M}$ and approaches the fixed point $(0,0)$ on $\partial\mathcal{M}$ as $x \to -\infty$. Moreover, as $x \to \Gamma_1(t)^-$, the left pulse solution leaves a fixed neighborhood of $\mathcal{M}$ near O_1. We recall from the above discussion that the point O_1 on $T_o(\hat{c}_1)$ corresponds precisely to the $\xi \to -\infty$ limit of the leading order fast (inner) solution v_0. Geometrically, it is the basepoint of a fast unstable fiber that lies in the transverse intersection of $W^U(\mathcal{M})$ and $W^S(\mathcal{M})$, as was shown in section 2.3.

The $\xi \to \infty$ limit of the fast (inner) solution is the point on $T_d(\hat{c}_1)$ labeled D_1 above, and it is the basepoint of the fast stable fiber that lies in the transverse intersection of $W^U(\mathcal{M})$ and $W^S(\mathcal{M})$. On all compact intervals in ξ, the left pulse of the slowly varying two-pulse solution lies close to (though not in) this transverse intersection.

The left and right pulses move when $\hat{c}_1(t)$ and $\hat{c}_2(t)$ are not identically zero, and hence their separation distance, $\Gamma_2(t) - \Gamma_1(t)$, changes in time. In particular, the given wave speed $\hat{c}_1$ determines the location of the point O_1, which in turn determines the points D_1, O_2, and O_2 sequentially, where

$$\begin{aligned} &O_1 : \ell^u \cap T_o(\hat{c}_1), \\ &D_1 : \mathcal{F}(\ell^u) \cap T_d(\hat{c}_1), \\ &O_2 : \mathcal{F}^{-1}(\ell^s) \cap T_o(\hat{c}_2), \\ &D_2 : \ell^s \cap T_d(\hat{c}_2). \end{aligned} \tag{3.1}$$

The ODE governing $\Gamma_2(t) - \Gamma_1(t)$ is then naturally obtained by imposing the leading order consistency condition that, at every instant of time, the difference $\Gamma_2(t) - \Gamma_1(t)$ equals the time of flight along the hyperbolic cosine orbit segment between the points D_1 and O_2 on $\mathcal{M}$.

3.3. Summary of the construction. In summary, the essential step of the analysis of the given reaction terms in (1.1) is to determine the geometry of $T_o(\hat{c})$, $T_d(\hat{c})$, ℓ^u, ℓ^s, $\mathcal{F}(\ell^u)$, and $\mathcal{F}^{-1}(\ell^s)$ on $\mathcal{M}$. With this in hand, one can then readily determine how many different types of pulses are possible and whether or not it is possible to construct repelling or attracting two-pulse solutions. We do this for various f and g in (1.1) in the next sections. Moreover, this method readily generalizes to asymmetric two-pulse solutions and to N-pulse solutions with $(N-1)$ segments near hyperbolic cosine solutions on $\mathcal{M}$, as is shown toward the end of this article.

Remark 3.1. A hard look at the leading order quasi-stationary solution constructed in this section reveals that it is not sufficiently smooth at $x = x_0$ due to the change in $\hat{c}$ at x_0 in (2.3). In particular, just as was observed in the construction of symmetric, slowly varying two-pulse solutions in the Gray–Scott model in [4], the third order (and higher order) derivatives of U do not vanish at $x = x_0$ as they should so that the full solution is symmetric. For example, the jump in U_{xxx} is $\mathcal{O}(\varepsilon^4)$ and hence truly of higher order. A similar smoothness problem is encountered for nonsymmetric two-pulse and N-pulse solutions at the points where the adjacent pulses are hooked up. However, we showed for the Gray–Scott model in section 3.4 of [4] that inclusion of the higher order terms beyond the leading order quasi-stationary approximation restores the smoothness in the third order derivatives and in all higher order odd derivatives. The lack of smoothness of the leading order quasi-stationary approximation

for the solutions studied here can be similarly ameliorated by inclusion of the higher order terms. We do not go into the details.

4. Symmetric, attracting, or repelling two-pulse solutions. In this section, we study symmetric, attracting, or repelling two-pulse solutions in systems of the form (1.1) for which

(i) $g'(u) \neq 0$ for all $u > 0$ and

(ii) the function $H(u) = 3f(u)/g^2(u) - \sqrt{\mu}u$ has one simple zero.

Under these conditions, the intersection of ℓ^u and $T_o(0)$ is transverse and consists of a single point; see (2.9) and (2.18). As a consequence, the PDE (1.1) possesses a stationary ($\hat{c} = 0$) one-pulse solution. See also section 7.1.

We construct slowly varying two-pulse solutions for which the slowly changing pulse velocities are equal in magnitude but opposite in sign at each instant of time t and for which the pulses either attract ($g'(u) > 0$) or repel ($g'(u) < 0$). In addition, we will see that there is an extremal allowable pulse speed (a minimum in the case of attracting pulses and a maximum in the case of repelling pulses) that arises naturally from the system geometry.

Conditions (i) and (ii) are formulated here mostly to facilitate the presentation of the geometric method. In the following sections, we will see that two-pulse solutions can also be constructed when $g'(u)$ has zeros, or when the function $H(u)$ has either no zeros or two (or more) zeros.

4.1. Singular two-pulse solutions. The singular two-pulse solutions are constructed following the blueprint developed in section 3.1. Consider the left pulse with peak at $x = \Gamma_1 < 0$ (where we have taken $x_0 = 0$ without loss of generality), and assume that the local maximum of u at the center of the pulse, denoted u^+, is given by some value satisfying

$$-\sqrt{\mu}u^+ < \sqrt{\mu}u^+ - \frac{6f(u^+)}{g^2(u^+)} < 0. \tag{4.1}$$

We note that Remark 4.1 provides the geometric reasons for the restriction (4.1).

The left pulse is backward asymptotic to $S = (0, 0, 0, 0)$. It has the following slow and fast segments (see also Figure 2.1):

- The left slow segment, which corresponds to the interval $(-\infty, \Gamma_1)$, is that portion of ℓ^u between S and the point O_1, which is the point in $\ell^u \cap T_o(\hat{c}_1)$ whose u-coordinate is given by the unique solution u^+ of

$$\sqrt{\mu}u = 2\hat{c}_1 \frac{g(u)}{g'(u)} + \frac{3f(u)}{g^2(u)}. \tag{4.2}$$

  Note that $\hat{c}_1$ is undetermined, as yet.
- The fast, homoclinic jump occurs at $x = \Gamma_1$, instantaneously on the outer scale x, and it is of infinite duration on the stretched ξ scale, with $\xi \in (-\infty, \infty)$. This fast jump begins at the point O_1 in $\ell^u \cap T_o(\hat{c}_1)$, where $O_1 = (u^+, p^+)$ and $p^+ = \varepsilon\sqrt{\mu}u^+$ by (2.9). The touchdown point of this fast jump is the point D_1 on $\mathcal{F}(\ell^u) \cap T_d(\hat{c}_1)$ with $u = u^+$. Specifically, $D_1 = (u^+, \varepsilon[\sqrt{\mu}u^+ - (6f(u^+)/g^2(u^+))])$, by (2.18) and (4.2) or by (2.19).
- The right slow segment, which corresponds to the interval $(\Gamma_1, 0]$, is the segment of hyperbolic cosine orbit on $\mathcal{M}$ that goes through D_1 up until it hits the u-axis at a point labeled $(u_{\min}, 0)$.

The phase space geometry reveals that, in this case, a good singular two-pulse solution can be formed by choosing the right pulse so that it is a reflection of the left pulse about $x = 0$. As a consequence, we have $\hat{c}_2 = -\hat{c}_1$. The singular solution for the right pulse has a left slow segment on $[0, \Gamma_2)$, where $\Gamma_2 = -\Gamma_1$, that is, the continuation of the above hyperbolic cosine orbit from $(u_{\min}, 0)$ to the point $O_2 = (u^+, \varepsilon[-\sqrt{\mu}u^+ + (6f(u^+)/g^2(u^+))])$, which is on both $T_o(\hat{c}_2)$ and $\mathcal{F}^{-1}(\ell^s)$; see (2.20). Finally, there is the fast jump at $x = \Gamma_2$ from the point O_2 to the point D_2 on ℓ^s in the phase space, followed by the right slow segment defined for (Γ_2, ∞) along ℓ^s from D_2 all the way back into S.

The results of section 3.2 now directly imply the existence of two-pulse solutions for $0 < \varepsilon \ll 1$, and these true solutions are close to the singular ($\varepsilon = 0$) two-pulse solutions just constructed.

Remark 4.1. The reason for the restriction (4.1) on the allowable u^+ values is intrinsic to the phase space geometry. The first landing point, D_1, which lies on $\mathcal{F}(\ell^u)$, must lie above ℓ^s and below the u-axis. Otherwise, the next slow segment lies outside of the wedge, and the solution cannot return to the $\{\hat{p} > 0\}$ half-plane, or the solution can never enter the $\{\hat{p} < 0\}$ half-plane. The restriction (4.1) states that u^+ should be such that $\mathcal{F}(\ell^u)$ is in between the positive u-axis and the ray $\hat{p} = -\sqrt{\mu}u$, which is ℓ^s, i.e., in that part of the wedge with negative $\hat{p}$-coordinate. As a consequence, D_1 must be a point on a hyperbolic cosine solution of the reduced slow system with negative $\hat{p}$-coordinate. It is also useful to note that, in the special case in which $f(0)/g^2(0) > 0$ and the intersection $\mathcal{F}(\ell^u) \cap \mathcal{F}^{-1}(\ell^s)$ is nonempty, the condition (4.1) can also be written as

$$\pi_u\left(\ell^u \cap T_o(0)\right) < u^+ < \pi_u(\mathcal{F}(\ell^u) \cap \mathcal{F}^{-1}(\ell^s)), \tag{4.3}$$

where π_u denotes the projection onto the u-coordinate.

4.2. The ODE for the pulse separation distance. In this section, we derive the implicit ODE for the separation distance between the pulses of the symmetric two-pulse solutions under consideration. From the definitions of the pulse positions, the distance between the two pulses in the lab frame (x-axis) is

$$\Delta\Gamma(t) = \Delta\Gamma(0) - 2\varepsilon^3 \int_0^t \hat{c}_1(s)ds, \tag{4.4}$$

where we have introduced $\Delta\Gamma(t) \equiv \Gamma_2(t) - \Gamma_1(t)$ as the distance between the two pulses and we have used $\hat{c}_2 = -\hat{c}_1$. Hence

$$\frac{d}{dt}\Delta\Gamma(t) = -2\varepsilon^3\hat{c}_1(t). \tag{4.5}$$

Moreover, instantaneously, at any t, the speed of the left pulse is given in terms of u^+ by

$$\hat{c}_1 = \left[\sqrt{\mu}u^+ - \frac{3f(u^+)}{g^2(u^+)}\right]\frac{g'(u^+)}{2g(u^+)}, \tag{4.6}$$

since the takeoff (or jump off) point O_1 for the fast jump lies in $\ell^u \cap T_o(\hat{c}_1)$; see (4.2). Therefore, plugging in the pulse speed (4.6) into the ODE (4.5), we find

$$\frac{d}{dt}\Delta\Gamma(t) = -\varepsilon^3\left[\sqrt{\mu}u^+ - \frac{3f(u^+)}{g^2(u^+)}\right]\frac{g'(u^+)}{g(u^+)}. \tag{4.7}$$

Next, we express the right member of this equation in terms of $\Delta\Gamma$, at least implicitly for the general $f(u)$ and $g(u)$ under consideration. From the geometry in the phase space, we see that the distance $\Delta\Gamma(t)$ equals the sum of the "times" of flight along the two hyperbolic cosine orbit segments on $\mathcal{M}$ between D_1 and $(u_{\min}, 0)$ and between $(u_{\min}, 0)$ and O_2, respectively. The leading order expression for this total "time" is found by examining the leading order ODEs for the dynamics on $\mathcal{M}$ written in terms of the fast "time" ξ,

$$\ddot{u} = \varepsilon^4 \mu u,$$

where we used (2.8) and dropped the last term because it is of higher order. Hence the general solution is

$$u(\xi) = Ae^{\varepsilon^2\sqrt{\mu}\xi} + Be^{-\varepsilon^2\sqrt{\mu}\xi}. \tag{4.8}$$

In turn, the coefficients A and B for the desired hyperbolic cosine orbit segment are determined by the condition that $(u(0), \dot{u}(0)/\varepsilon) = D_1$. Hence

$$\begin{aligned} A + B &= u^+, \\ \sqrt{\mu}\,(A - B) &= \sqrt{\mu}u^+ - \frac{6f(u^+)}{g^2(u^+)}, \end{aligned}$$

which implies that

$$A = u^+ - \frac{3f(u^+)}{\sqrt{\mu}g^2(u^+)} \quad \text{and} \quad B = \frac{3f(u^+)}{\sqrt{\mu}g^2(u^+)}. \tag{4.9}$$

The other condition that has to be satisfied is that, when the total "time" of flight ξ_T along these hyperbolic orbit segments satisfies $\varepsilon\xi_T = \Delta\Gamma$, the solution $u(\xi)$ has to be at the point O_2. Looking at $u_\xi(\xi_T)$, we find

$$\varepsilon^2\sqrt{\mu}(Ae^{\varepsilon^2\sqrt{\mu}\xi_T} - Be^{-\varepsilon^2\sqrt{\mu}\xi_T}) = \varepsilon^2\left(-\sqrt{\mu}u^+ + \frac{6f(u^+)}{g^2(u^+)}\right).$$

By setting $z = e^{\varepsilon^2\sqrt{\mu}\xi_T}$, rewriting this equation as a quadratic in z, using (4.9), and choosing the positive solution ($z_+ = B/A$, which is known in terms of u^+), we obtain

$$e^{-\varepsilon\sqrt{\mu}\Delta\Gamma(t)} = \frac{\sqrt{\mu}u^+ - \frac{3f(u^+)}{g^2(u^+)}}{\frac{3f(u^+)}{g^2(u^+)}}. \tag{4.10}$$

Finally, we use (4.10) to replace the term in square brackets in (4.7):

$$\frac{d}{dt}\Delta\Gamma(t) = -3\varepsilon^3\frac{f(u^+)g'(u^+)}{g^3(u^+)}e^{-\varepsilon\sqrt{\mu}\Delta\Gamma(t)}. \tag{4.11}$$

The ODE (4.11) is the desired ODE for the separation distance $\Delta\Gamma(t) = \Gamma_2(t) - \Gamma_1(t)$. The value of u^+ is given implicitly by (4.10), i.e., by

$$\mathcal{G}(u^+) = \frac{e^{-\varepsilon\sqrt{\mu}\Delta\Gamma} + 1}{\sqrt{\mu}}, \tag{4.12}$$

as long as this root exists, where $\mathcal{G}$ is the single-valued function defined by

$$\mathcal{G}(u^+) \equiv \frac{u^+g^2(u^+)}{3f(u^+)}. \tag{4.13}$$

4.3. Interpretation of the implicit ODE (4.11). Since f and g are strictly positive by assumption, the sign of $\frac{d}{dt}\Delta\Gamma$ is determined by that of $g'(u)$. Moreover, $g'(u)$ is sign-definite in the analysis of this section because we assumed that $g'(u) \neq 0$ for all $u > 0$. Therefore, we conclude from (4.11) that

$$\begin{aligned} &\text{if } g'(u) > 0, \quad \text{then } \frac{d}{dt}\Delta\Gamma < 0, \text{and the pulses attract;} \\ &\text{if } g'(u) < 0, \quad \text{then } \frac{d}{dt}\Delta\Gamma > 0, \text{and the pulses repel.} \end{aligned} \tag{4.14}$$

The ODE (4.11) also yields an extremal value of the pulse speed. In particular, the left member of (4.11) equals $-2\varepsilon^3\hat{c}_1$ by the definitions of Γ_1 and Γ_2 and by the fact that $\hat{c}_2 = -\hat{c}_1$ here. Therefore, since the right member has an extremum when $\Gamma_2 = \Gamma_1$, i.e., $\Delta\Gamma = 0$, we find that an extremum of $\hat{c}_1$ occurs at $\sqrt{\mu}u^+g'(u^+)/(4g(u^+))$. This extremum is a maximum when $g'(u) < 0$ and a minimum when $g'(u) > 0$. Also, we note that $\hat{c}(t)$ might have additional (local) extrema; see section 6.

Finally, in the limit $\Delta\Gamma \gg 1$, the ODE for the separation distance between the two pulses in this case is the same as that one would find from weak interaction theory; i.e., to leading order

$$\frac{d}{dt}\Delta\Gamma(t) = C_1 e^{-C_2\Delta\Gamma(t)}$$

for some positive constants C_1 and C_2; see [12, 14].

This completes our analysis of symmetric, slowly varying, two-pulse solutions of (1.1) under conditions (i) and (ii).

5. Examples. In this section, we consider three explicit examples of systems in which semistrong pulse interactions occur and analyze the dynamics of symmetric two-pulse solutions constructed by the methods developed in sections 3 and 4.

The first example has a purely mathematical character. We choose $f(U)$ and $g(U)$ in (1.1) such that the computational effort to determine an explicit version of the ODE (4.11) for $\Delta\Gamma(t)$ is minimal. The other two examples are more physically motivated. As stated in the introduction, both systems are closely related to (and contain as a special case) the well-studied Gierer–Meinhardt equation, and they both show that semistrong pulse interactions can generate unexpected phenomena, such as finite-time blowup.

5.1. An elementary mathematical example. The first example is provided by the elementary mathematical case of $f(u) = \frac{1}{3}g^2(u)$ and $g(u) = e^{\frac{2u}{\gamma}}$, with $\gamma \neq 0$. Here, $f(u)$ and $g(u)$ are chosen such that the quotients $g(u)/g'(u)$ and $3f(u)/g^2(u)$ that appear throughout the analysis of the general case reduce to constants. As a consequence, $T_o(0)$, $T_d(0)$, $\mathcal{F}(\ell^u)$, and $\mathcal{F}^{-1}(\ell^s)$ are all given by straight lines. The ODE (4.11) becomes

$$\frac{d}{dt}\Delta\Gamma = -\varepsilon^3\frac{2}{\gamma}e^{-\varepsilon\sqrt{\mu}\Delta\Gamma} \tag{5.1}$$

with the restriction that $0 < \gamma\hat{c}_1 \leq 1$. This restriction follows necessarily from the condition $u^+ < 2/\sqrt{\mu}$ that arises from the phase space geometry, where $2/\sqrt{\mu} = \pi_u(\mathcal{F}(\ell^u) \cap \mathcal{F}^{-1}(\ell^s))$; see (4.1) and Figure 2.1. It directly yields the maximum wave speed $|\hat{c}_1| \leq 1/|\gamma|$.

If $\gamma > 0$, it is clear from (5.1) that $\Delta\Gamma(t)$ decreases and the pulses attract. In addition, their speeds $\hat{c}_1 = -\hat{c}_2$ increase algebraically in time according to the ODE

$$\frac{d}{dt}\hat{c}_1 = 2\varepsilon^4\sqrt{\mu}\hat{c}_1^2$$

up to the maximum wave speed $\hat{c}_1 = 1/\gamma$. At this point, the interaction becomes strong since not even the V-component is near zero in between the pulses anymore, and hence the interaction can no longer be considered to be semistrong. If, on the other hand, $\gamma < 0$, then $\hat{c}_1 < 0$ so that the pulses are repelling. Moreover, $|\hat{c}_1|$ decreases to zero algebraically in time.

The ODE (5.1) for the semistrong interaction of pulses in this symmetric case is identical to that obtained in the weak interaction limit. However, the semistrong analysis also yields the upper bound, $|\hat{c}_1| \leq 1/|\gamma|$, and it is valid for shorter distances $\Delta\Gamma$ between the pulses.

5.2. A modified Gierer–Meinhardt equation with finite-time blowup. Next, we consider the more realistic example of $f(u) \equiv 1$ and $g(u) = (1/u) + \alpha$, with $\alpha \geq 0$ since $g(U)$ in (1.1) must be positive; see, however, Remark 5.2. Thus (1.1) becomes a modified Gierer–Meinhardt equation,

$$\left\{ \begin{array}{rcl} \varepsilon^2 U_t &=& U_{xx} - \varepsilon^2\mu U + V^2, \\ V_t &=& \varepsilon^2 V_{xx} - V + (\frac{1}{U} + \alpha)V^2, \end{array} \right. \tag{5.2}$$

in which α plays the role of (an additional) bifurcation parameter. This equation reduces to the classical Gierer–Meinhardt equation if $\alpha = 0$; recall [7, 21]. Moreover, $g'(u) < 0$ for all $u > 0$ so that the pulses in symmetric two-pulse solutions are repelling for any α, including the classical Gierer–Meinhardt case $\alpha = 0$, by the theory presented in section 4.

5.2.1. The ODE for $\Delta\Gamma(t)$. It follows from (2.18), (2.19), and (2.20) that

$$T_o(\hat{c};\alpha), T_d(\hat{c};\alpha): \quad \hat{p} = -2\hat{c}u(\alpha u + 1) \pm \frac{3u^2}{(\alpha u + 1)^2}$$

and

$$\mathcal{F}(\ell^u), \mathcal{F}^{-1}(\ell^s): \quad \hat{p} = \pm\sqrt{\mu}u \mp \frac{6u^2}{(\alpha u + 1)^2}.$$

First, we observe that this equation can have two stationary, homoclinic, one-pulse solutions since the equation $\alpha^2u^2 + (2\alpha - 3/\sqrt{\mu})u + 1 = 0$, which is obtained from $T_o(0;\alpha) \cap \ell^u$, has two (positive) solutions for

$$0 < \alpha < \alpha_{bu} = \frac{3}{4\sqrt{\mu}}. \tag{5.3}$$

See also Remark 5.3. As $\alpha \to 0$, one of these pulse solutions becomes unbounded, and the other one merges with the (uniquely determined) one-circuit homoclinic pulse solution of the (classical) Gierer–Meinhardt equation [7]. In the opposite limit as $\alpha \uparrow \alpha_{bu}$, the pulses merge in a saddle-node bifurcation of homoclinic orbits.

The intersection $\mathcal{F}(\ell^u) \cap \mathcal{F}^{-1}(\ell^s)$ also consists of up to two points, and hence the condition (4.1) can yield up to two intervals of existence. In this section, we focus on the interval that corresponds to two-pulse solutions that merge with two-pulse solutions of the Gierer–Meinhardt equation in the limit $\alpha \to 0$ since these two-pulse solutions can be expected to

be stable. (These two-pulse solutions are associated to the stationary pulse solution of the Gierer–Meinhardt equation, and these pulses are stable if μ is above a certain critical value associated to a Hopf bifurcation [7].) We shall see that two-pulse solutions exist beyond α_{bu}, i.e., for values of α for which there are no stationary pulses. This is not necessarily surprising since the construction of two-pulse solutions is based on the intersection(s) of $T_o(\hat{c};\alpha)$ and ℓ^u for $\hat{c} \neq 0$. This intersection can of course be nonempty even if $T_o(0;\alpha) \cap \ell^u = \emptyset$. Furthermore, $\mathcal{F}(\ell^u)$ lies in the $\{\hat{p} > 0\}$ half-plane for $\alpha > 3/(2\sqrt{\mu}) = 2\alpha_{bu}$; recall (5.3). Hence it is not possible to construct these types of two-pulse solutions for $\alpha > 2\alpha_{bu}$; see Remark 4.1.

The ODE for $\Delta\Gamma(t)$ in this example may be determined directly by substituting the choices of f and g into (4.11). We obtain

$$\frac{d}{dt}\Delta\Gamma = 3\varepsilon^3 \frac{u^+}{(\alpha u^+ + 1)^3} e^{-\varepsilon\sqrt{\mu}\Delta\Gamma}, \tag{5.4}$$

where $0 < \alpha < 2\alpha_{bu}$, and we note that, by (4.12) and (4.13), u^+ is related to $\exp(-\varepsilon\sqrt{\mu}\Delta\Gamma)$ through

$$\frac{e^{-\varepsilon\sqrt{\mu}\Delta\Gamma} + 1}{\sqrt{\mu}} = \frac{(\alpha u^+ + 1)^2}{3u^+} = \mathcal{G}(u^+),$$

where we recall the definition of $\mathcal{G}$ given in (4.13). A little algebra yields

$$\frac{1}{\alpha u^+ + 1} = \frac{1}{2} - \frac{1}{2}\sqrt{1 - \frac{4\alpha}{3\mathcal{G}}}.$$

Hence the ODE (5.4) becomes an explicit ODE for $\Delta\Gamma(t)$,

$$\frac{d}{dt}\Delta\Gamma = \varepsilon^3\sqrt{\mu}\frac{\sqrt{1 - \frac{\alpha}{\alpha_{bu}} + e^{-\varepsilon\sqrt{\mu}\Delta\Gamma}}}{(1 + e^{-\varepsilon\sqrt{\mu}\Delta\Gamma})^{3/2}} e^{-\varepsilon\sqrt{\mu}\Delta\Gamma}. \tag{5.5}$$

Note that in the classical Gierer–Meinhardt equation, i.e., $\alpha = 0$ in (5.2), the ODE for the evolution of symmetric two-pulse solutions reduces to

$$\frac{d}{dt}\Delta\Gamma = \varepsilon^3\sqrt{\mu}\frac{e^{-\varepsilon\sqrt{\mu}\Delta\Gamma}}{1 + e^{-\varepsilon\sqrt{\mu}\Delta\Gamma}}. \tag{5.6}$$

5.2.2. Pulse dynamics governed by (5.5) and the blowup time. For parameter values $0 < \alpha < \alpha_{bu}$, the solutions $\Delta\Gamma(t)$ of the ODE (5.5) are defined for all $t > 0$ because $\exp(-\varepsilon\sqrt{\mu}\Delta\Gamma) \in (0,1)$. The ODE (5.5) describes a pair of symmetric pulses which always move away from each other with decreasing speed.

For parameter values $\alpha_{bu} \leq \alpha < 2\alpha_{bu}$, the ODE (5.5) also governs the evolution of symmetric two-pulse solutions even though there is no stationary, homoclinic, one-pulse solution for $\alpha \geq \alpha_{bu}$. However, the ODE is well defined now only for a finite time and only for $\Delta\Gamma(t)$ not too large. More precisely, in order for the ODE (5.5) to be well defined, $\Delta\Gamma(t)$ must be less than the critical pulse separation distance,

$$\Delta\Gamma_{bu} = \frac{-1}{\varepsilon\sqrt{\mu}} \ln\left(\frac{\alpha}{\alpha_{bu}} - 1\right),$$

which is the value of $\Delta\Gamma(t)$ when the term under the square root in (5.5) vanishes.

Let us take a more in-depth look at two pulses that, at $t = 0$, are less than a distance $\Delta\Gamma_{bu}$ apart, i.e., $\Delta\Gamma(0) < \Delta\Gamma_{bu}$. As just shown, the dynamics of these pulses is governed by (5.5). Nevertheless, (5.5) shows that these pulses move away from each other so that $\Delta\Gamma(t)$ increases. It follows that there is a time $t = t_{bu}$, which depends on the initial conditions, at which $\Delta\Gamma = \Delta\Gamma(t_{bu}) = \Delta\Gamma_{bu}$. Beyond t_{bu}, it is no longer possible to have two-pulse orbits (almost) homoclinic to the slow manifold $\mathcal{M}$. The methods developed in this article cannot be used to describe the pulses after the pulses reach the critical separation distance $\Delta\Gamma_{bu}$.

5.2.3. Finite-time blowup and a codimension two self-replication/blowup bifurcation point. Numerical simulations show that the theory works very well qualitatively and quantitatively. In Figure 5.1, we show the evolution of a symmetric two-pulse solution of (5.2) with $\varepsilon^2 = 0.01$, $\mu = 5$, and $\alpha = 0.342$; thus, by (5.3), $\alpha \in (\alpha_{bu}, 2\alpha_{bu})$, where $\alpha_{bu} \approx 0.335$. The evolution of the pulses is slow up to $t = t_{bu}$; in fact, the speed of the pulses reduces to zero as $t \to t_{bu}$ (5.2). Then, as soon as t passes through t_{bu}, one of the pulses starts to grow rapidly, both in its U-component and in its V-component. Both components blow up in finite time. The solution to (5.2) has become unbounded on a localized spatial domain for t slightly above t_{bu}.

This finite-time blowup behavior occurs generically in (5.2) for α and μ such that $\alpha \in (\alpha_{bu}, 2\alpha_{bu})$ with suitably chosen initial conditions—see below. Only one of the pulses blows up; the other one is almost immediately overtaken by the exploding one. The distinction between blowing up and being overtaken seems to depend on (extremely small) asymmetric effects in the sense that an initially (i.e., for $t < t_{bu}$) negligible difference between the amplitude of the two pulse is strongly magnified as soon as t passes through t_{bu}.

The roots of this dynamic finite-time blowup behavior lie in the bifurcation of the stationary, solitary, homoclinic, one-pulse solution to (5.2), which exists and is stable for $\alpha < \alpha_{bu}$. For $\alpha = \alpha_{bu} - \sigma$ with $0 < \sigma \ll 1$, the solitary, one-pulse solution is attracting, whereas for $\alpha = \alpha_{bu} + \sigma$, initial conditions coincident with—or sufficiently close to—the form of the one-pulse solution for $\alpha = \alpha_{bu} - \sigma$ blow up in finite time in (5.2). However, this is not the case for all μ. As soon as μ becomes $\mathcal{O}(1/\varepsilon^4)$—see [10] and Remark 5.4—the pulse might undergo a self-replication bifurcation instead of the finite-time blowup bifurcation; i.e., the pulse might split into a (symmetric) pair of traveling pulses that eventually split again, etc. Thus the self-replication bifurcation also occurs in the modified Gierer–Meinhardt equation (5.2). As explained in [10], self-replication of pulses is a generic phenomenon that is not unique to the Gray–Scott equation [3, 4, 5, 9, 28, 31, 34, 39, 40, 43, 44]. Both bifurcations determine a curve in the (μ, α) parameter plane. It is found (numerically) for $\varepsilon^2 = 0.1$ that these two curves intersect at a codimension two finite-time self-replication/blowup bifurcation point at $(\mu, \alpha) \approx (22, 0.06)$. This last statement is based on numerical observation; however, the methods developed in [7] can be used to obtain rigorous results. See also section 7.1.

Remark 5.1. The ODE (5.5) for $\Delta\Gamma(t)$ (in this case of symmetric pulses) has a natural counterpart in an ODE for $\hat{c} = \hat{c}(t) = \pm\hat{c}_{1,2}(t)$ that may be derived by substituting the general relation (4.5) between $\frac{d\Delta\Gamma}{dt}$ and $\hat{c}$ into the left member of (5.5). However, the expression for $\hat{c}$ determined in this way is in terms of $Z = \exp(-\varepsilon\sqrt{\mu}\Delta\Gamma)$ (recall (4.5)). Hence one first needs to determine an expression for Z in terms of $\hat{c}$ and then to invert that expression before one

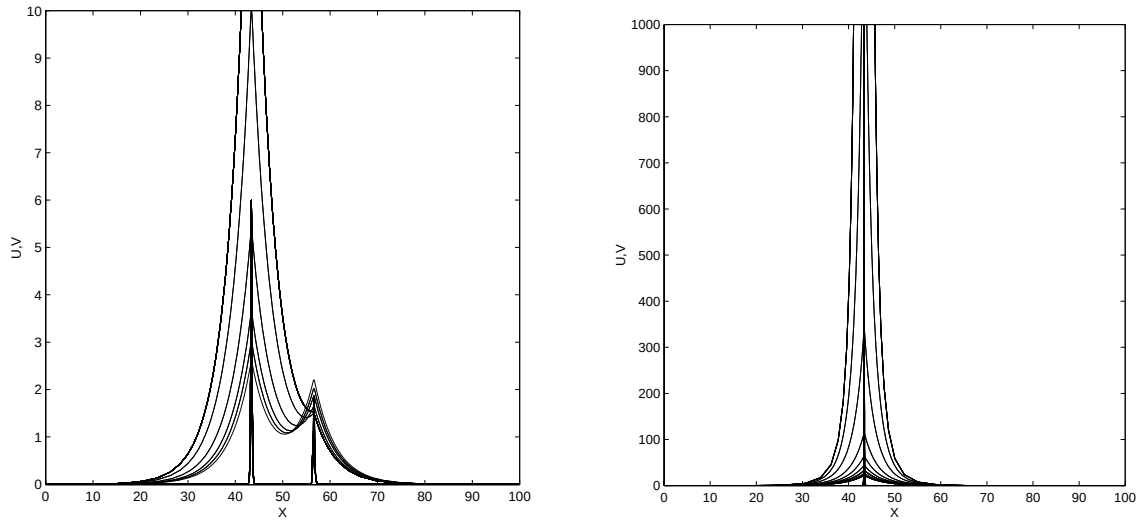

Figure 5.1. *Evolution of a symmetric two-pulse solution of the modified Gierer–Meinhardt equation* (5.2) *with* $\varepsilon = 0.1$, $\mu = 5$, *and* $\alpha = 0.342$. *Here,* $\alpha \in (\alpha_{bu}, 2\alpha_{bu})$, *but close to* $\alpha_{bu} \approx 0.335$; *see section* 5.3.2. *In the left frame, the sequence of times is* $t = 0, 40, 50, 55, 57, 57.6$, *where* $t = 0$ *corresponds (approximately) to the time* ($t = t_{bu}$) *at which the symmetric two-pulse solution reaches the critical separation distance* $\Delta\Gamma_{bu}$. *In the right frame, the results of continuing the same simulation are presented for the sequence of times* $t = 57.8, 57.9, 58.0, 58.1, 58.2, 58.3, 58.4, 58.45, 58.47$. *Blowup in both* U *and* V *occurs appears to occur at* $t \approx 58.472$ *(and of course the actual value may vary slightly depending on implementation and hardware). Again, we used* 201 *grid points and homogeneous Neumann boundary conditions.*

can derive the equation for $d\hat{c}/dt$ from (5.5). Thus, for general α, one has to solve a cubic equation in Z. This is an unpleasant task, and the outcome will not give much additional insight. However, there are two special values of α, the Gierer–Meinhardt case $\alpha = 0$ and the bifurcation case $\alpha = \alpha_{bu}$, for which the cubic equation reduces to a much simpler equation. For the Gierer–Meinhardt equation ($\alpha = 0$), we find that the equation for the speed of the pulses is given by

$$\frac{d}{dt}\hat{c} = 2\varepsilon^4(\sqrt{\mu} + 2\hat{c})\hat{c}^2.$$

Also, for the bifurcation case, $\alpha = \alpha_{bu}$, we find

$$\frac{d}{dt}\hat{c} = 2\varepsilon^4\mu^{1/6}(\mu^{1/3} - (2\hat{c})^{2/3})\hat{c}^2.$$

Remark 5.2. In this article, we assume that $g(U)$ in (1.1) is positive so that homoclinic solutions can exist in the fast reduced limit problem (2.5). This does not rule out examining (5.2) for $\alpha < 0$. In fact, for $\alpha < 0$ we can (only) consider U such that $g(U) \geq 0$; i.e., we consider U values that are small enough. In that case, it is also found that the stationary, solitary, homoclinic pulse of the Gierer–Meinhardt equation ($\alpha = 0$ in (5.2)) persists, as is the case for $\alpha > 0$. The fate of this pulse for decreasing α of course also depends on the other parameters (ε and μ). For instance, it is found numerically for $\varepsilon^2 = 0.01$ and $\mu = 5.0$ that the pulse remains stable up to $\alpha \approx -400$ (!). For such values of α, the pulse has indeed become

tiny ($0 < U < 0.0025$). As α decreases even further, the pulse undergoes the self-replication bifurcation, which leads to a spatially periodic array of "midget pulses."

Remark 5.3. Since $T_o(0;\alpha)$ and ℓ^u can have two intersection points, it is also possible to construct pairs of *asymmetric* pulses. The geometric construction is straightforward; however, the derivation of the ODE for the dynamics of the pulses is quite cumbersome and does not give additional insight. Interestingly, though, the asymmetric solution approaches the symmetric two-pulse solution as the parameter α approaches α_{bu}. So there may be a connection between the asymmetry that appears in the simulations reported here, which are for a value of α very close to, though above, α_{bu}. Finally, we do not expect that these asymmetric two-pulse solutions are stable.

Remark 5.4. It has been proved in [10] that there is a bifurcation in the Gierer–Meinhardt equation ($\alpha = 0$ in (5.2)) that annihilates the solitary homoclinic pulse for $\mu = \mathcal{O}(1/\varepsilon^4)$. This bifurcation initiates the self-replication process. A similar analytical result can be obtained for the modified Gierer–Meinhardt equation (5.2) introduced above and for the modified Gierer–Meinhardt equation (5.7) introduced below.

5.3. A modified Gierer–Meinhardt equation with asymptotically large pulses. Finally, we consider another small modification of the classical Gierer–Meinhardt equation

$$\left\{\begin{array}{rcl} \varepsilon^2 U_t &=& U_{xx} - \varepsilon^2 \mu U + V^2, \\ V_t &=& \varepsilon^2 V_{xx} - V + (\frac{1}{U} + \frac{\beta}{\sqrt{U}})V^2; \end{array}\right. \tag{5.7}$$

i.e., we have set $f(U) \equiv 1$ and $g(U) = (1/U) + (\beta/\sqrt{U})$ in (1.1), where $\beta \geq 0$ is the new bifurcation parameter. In the special case $\beta = 0$, (5.7) is again the Gierer–Meinhardt equation.

5.3.1. Blowup of stationary, homoclinic, one-pulse solutions. We immediately obtain

$$T_o(\hat{c};\beta), T_d(\hat{c};\beta): \quad \hat{p} = -2\hat{c}u\frac{1+\beta\sqrt{u}}{1+\frac{1}{2}\beta\sqrt{u}} \pm \frac{3u^2}{(1+\beta\sqrt{u})^2}$$

and the related expressions for $\mathcal{F}(\ell^u)$ and $\mathcal{F}^{-1}(\ell^s)$. For

$$0 \leq \beta < \beta_\infty = \sqrt{\frac{3}{\sqrt{\mu}}}, \tag{5.8}$$

there is a unique intersection of $T_o(0;\beta)$ and ℓ^u with u-coordinate

$$u = \frac{1}{(\beta_\infty - \beta)^2}. \tag{5.9}$$

Thus there is a uniquely determined stationary, homoclinic, one-pulse solution for $0 \leq \beta < \beta_\infty$. Moreover, the formula (5.9) reveals that the amplitude of this solution diverges as $\beta \uparrow \beta_\infty$; i.e., the blowup is determined *analytically* in this example. This situation contrasts with the situation for the previous example, where the amplitude approaches a finite number ($\frac{3}{4\sqrt{\mu}}$) as $\alpha \to \alpha_{bu}$ and the blowup was observed numerically.

Here the analysis is again confirmed by the numerical simulations. The homoclinic pulse that corresponds to $T_o(0;\beta) \cap \ell^u$ is asymptotically stable up to $\beta = \beta_\infty$. Its amplitude also

agrees (to leading order) with (5.9): for $\varepsilon = 0.1$ and $\mu = 5.0$, i.e., $\beta_\infty \approx 1.158$ (5.8), we observe, for instance, in the simulations that the amplitude of the U-component of the pulse is approximately 5.0 for $\beta = 0.7$, while (5.9) gives 4.76. Of course, the error grows as $\beta \to \beta_\infty$: for $\beta = 1.1$, i.e., $\beta_\infty - \beta \approx 0.058$, the height of the U-component of the pulse is ≈ 337.8 in the simulation (see also Figure 5.2), while (5.9) yields ≈ 294.2. Nevertheless, the relative error is still of $\mathcal{O}(\varepsilon)$ near the singular limit.

5.3.2. Symmetric two-pulse solutions: The ODE for $\Delta\Gamma(t)$ and an analytical expression for finite-time blowup. The derivation of the ODE for $\Delta\Gamma(t)$, the distance between the pulses of a two-pulse solution, proceeds directly along the lines of the general theory of section 4. We find

$$\frac{d}{dt}\Delta\Gamma = \varepsilon^3\sqrt{\mu}\frac{\left[\sqrt{1+e^{-\varepsilon\sqrt{\mu}\Delta\Gamma}} - \frac{\beta}{2\beta_\infty}\right]}{(1+e^{-\varepsilon\sqrt{\mu}\Delta\Gamma})^{3/2}}e^{-\varepsilon\sqrt{\mu}\Delta\Gamma}, \tag{5.10}$$

which also reduces to (5.6) in the Gierer–Meinhardt limit $\beta = 0$.

As in the previous example, it is possible to construct symmetric two-pulse solutions beyond the critical value β_∞. The upper bound on β is determined by the observation that two-pulse solutions can only be constructed for u values such that the corresponding point on $\mathcal{F}(\ell^u)$ lies below the u-axis. Hence it follows that two-pulse solutions exist for $0 \le \beta < \sqrt{2}\beta_\infty$. Note that this second critical value of β, $\sqrt{2}\beta_\infty$, does not show up explicitly in the ODE (5.10). We shall discuss the implications of this below.

The amplitude u^+ of the U-component of the pulse is given by

$$u^+ = \frac{1}{(\beta_\infty\sqrt{1+e^{-\varepsilon\sqrt{\mu}\Delta\Gamma}} - \beta)^2}; \tag{5.11}$$

see (4.12) and (4.13). This relation confirms the necessity of the condition $\beta < \sqrt{2}\beta_\infty$. Thus u^+ remains bounded for all (finite) time as long as $\beta \le \beta_\infty$, and the ODE (5.10) is well defined for all time.

In contrast, for $\beta_\infty < \beta < \sqrt{2}\beta_\infty$, the ODE (5.10) is only well defined for

$$\Delta\Gamma < \Delta\Gamma_\infty = \frac{-1}{\varepsilon\sqrt{\mu}}\ln\left(\frac{\beta^2}{\beta_\infty^2} - 1\right).$$

Thus, for $\beta_\infty < \beta < \sqrt{2}\beta_\infty$, the ODE (5.10) governs the dynamics of two-pulse solutions that are close enough at $t = 0$; i.e., $\Delta\Gamma(0)$ must be less than $\Delta\Gamma_\infty$. Since $\Delta\Gamma(t)$ is an increasing function of time (5.10), there must be a critical time t_∞ at which $\Delta\Gamma(t_\infty) = \Delta\Gamma_\infty$. Moreover, it is clear from (5.11) that the amplitude of the pulse diverges as t approaches t_∞. Thus this second modified Gierer–Meinhardt equation (5.7) also exhibits finite-time ($t = t_\infty$) blowup, and in this example the blowup can be studied analytically. Finally, if $\Delta\Gamma(0) > \Delta\Gamma_\infty$, then the pulses blow up immediately by the same process that causes the blowup of the stationary pulse for $\beta \ge \beta_\infty$.

At first sight, the dynamics of pulses in (5.7) seems to be essentially the same as in (5.2). However, there are three crucial differences, two of which emerge from the analysis and a third one that is observed in the numerical simulations, which will be discussed below. First, as

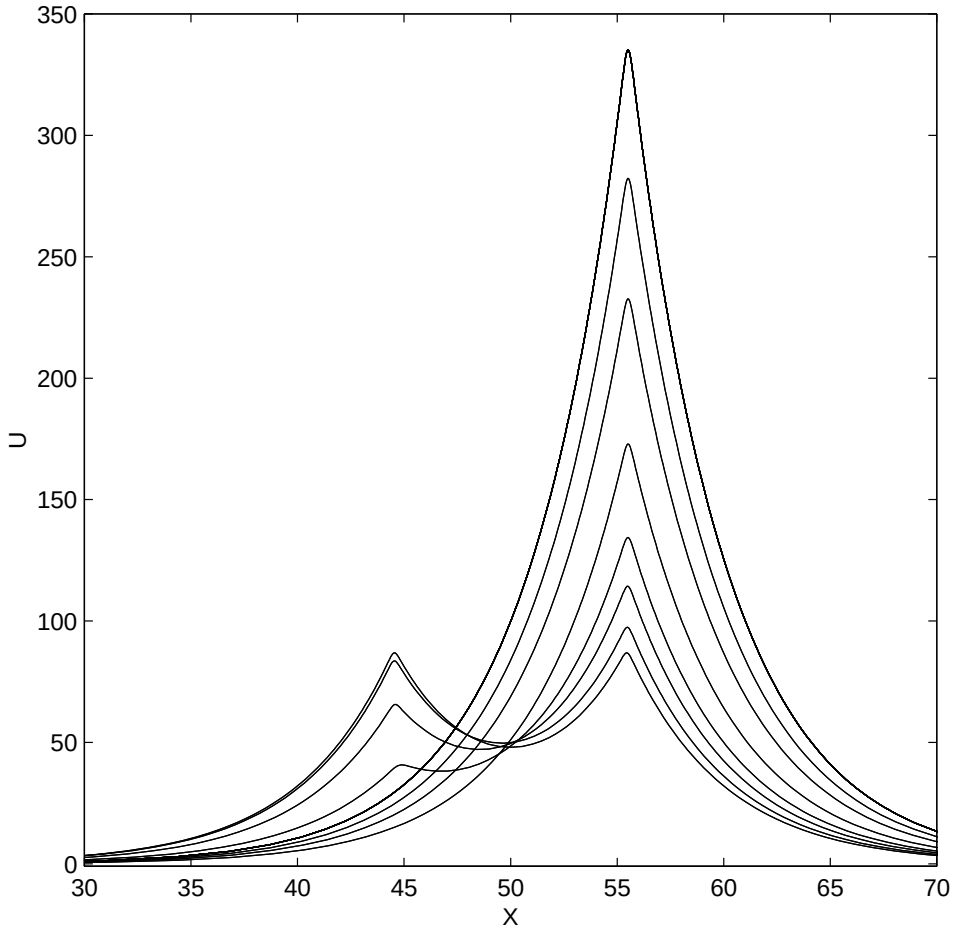

Figure 5.2. *Symmetry-breaking in the evolution of the U-component of an initially symmetric, slowly varying, two-pulse solution of the second modified Gierer–Meinhardt equation (5.7) with $\varepsilon^2 = 0.01$, $\mu = 5$, and $\beta = 1.1$. The symmetry-breaking bifurcation is observed in this simulation since $\Delta\Gamma(0) < \Delta\Gamma_{sb}$. See section 5.3.3. The time steps are $t = 0, 60, 68, 72, 76, 82, 90, \infty$, where again we set $t = 0$ at (approximately) the last time ($t = t_\infty$) at which a symmetric two-pulse solution exists. (The left pulse has its maximum value for the sequence of times shown here, while the right pulse has its minimum.) At $t = 60$, the asymmetry has become noticeable, and it is growing quickly. At $t = 72$, the left pulse has almost disappeared, and it is no longer visible at $t = 76$. The right pulse then grows even more quickly, and at $t = 90$ it is close to its asymptotic value ($t \to \infty$), which corresponds to the largest peak shown here. This simulation was also done with 201 grid points and homogeneous Neumann boundary conditions.*

was already noted, the finite-time blowup in this case can be fully understood by the analysis, unlike in the previous example. Here, the blowup occurs at $t = t_\infty$ so that the process can be described in full analytical detail, whereas in the previous example the finite-time blowup mechanism starts beyond the critical time t_{bu}. Second, there is a difference in the dynamics of the pulses at (or near) the critical time, t_{bu} or t_∞, respectively. In the previous example, the speed of the pulses approaches 0 as $t \to t_{bu}$. Here, the critical upper bound $\sqrt{2}\beta_\infty$ on β does not show up explicitly in the ODE (5.10). As a consequence, the speed of the pulses

approaches a well-defined limit as $t \to t_\infty$, namely,

$$|\hat{c}_\infty| = \frac{1}{4}\sqrt{\mu}\left(\frac{\beta^2}{\beta_\infty^2} - 1\right),$$

where we have used (4.5).

5.3.3. Stability and a symmetry-breaking bifurcation. We have based the two modified Gierer–Meinhardt examples of sections 5.2 and 5.3 on recently obtained results on the spectral stability of the homoclinic one-pulse solution in the Gierer–Meinhardt equation ((5.2), (5.7) with $\alpha, \beta = 0$); see [7]. Both pulses of the two-pulse solutions approach a single-pulse homoclinic solution of the Gierer–Meinhardt equation as $t \to \infty$ and $\alpha, \beta \to 0$. This gives a heuristic argument by which one can expect to see stable two-pulse solutions in the modified systems (5.2) and (5.7). It has been shown in [3, 4] that this argument works in the case of the Gray–Scott equation. Numerical simulations for the previous example suggest that the argument is also valid here. Moreover, the simulations also confirm the persistence of the stability beyond $\beta = 0$ for the stationary pulses. Of course, neither of these observations prove the stability.

On the contrary, the numerical simulations show that one cannot expect to fully understand the semistrong dynamics of the two-pulse solutions in (5.7) even with the combination of the existence analysis developed in this article and the stability results for the stationary homoclinic pulse.

We have performed numerical simulations of two-pulse solutions in (5.7) for $\varepsilon = 0.1$ and $\mu = 5.0$. (Note that the homoclinic pulse in the Gierer–Meinhardt ($\beta = 0$) equation has been proved to be stable for $\mu > \mu_{\text{Hopf}} \approx 0.36 + \mathcal{O}(\varepsilon)$.) Although we have already seen that the stationary pulses are stable up to $\beta = \beta_\infty$, which is approximately 1.158 by (5.8), we observed that the two-pulse solution undergoes a symmetry-breaking destabilizing bifurcation at $\beta = \beta_{sb} \approx 0.9 < \beta_\infty$. As long as $\beta < \beta_{sb}$, the two-pulse solution travels and grows according to (5.10) and (5.11). By contrast, for $\beta > \beta_{sb}$, the dynamics of the two-pulse solution depends crucially on the distance $\Delta\Gamma(0)$ between the pulses at $t = 0$. If $\Delta\Gamma(0)$ is large enough, i.e., if the system is close to the weak interaction limit and both pulses are sufficiently close to the solitary homoclinic pulse, then the pulses behave exactly as for $\beta < \beta_{sb}$. Note that this implies that the symmetry-breaking bifurcation is caused by the semistrong interactions. On the other hand, if $\Delta\Gamma(0)$ is below a certain critical value $\Delta\Gamma_{sb} = \Delta\Gamma_{sb}(\beta)$, then the pulses still evolve according to (5.10), but initially negligible differences between the heights of the two pulses increase (on a certain intermediate time scale). After a certain critical time, the smallest of the two pulses is overtaken completely by the larger one. The speed of the resulting pulse decreases to zero, and the end product of the symmetry-breaking bifurcation is a stable solitary pulse (see Figure 5.2). The numerics also show that the critical distance $\Delta\Gamma_{sb}(\beta)$ diverges rapidly as β approaches β_∞. The initial separation $\Delta\Gamma(0)$ must be so large for $\beta = 1.1$—recall that $\beta_\infty \approx 1.158$—that the interaction between the pulses indeed has become extremely weak. Thus we conclude that the predicted finite-time blowup does not occur due to the destabilizing symmetry-breaking effects. However, the appearance of the destabilizing bifurcation is expected to depend on the parameters μ and β. It is possible that the finite-time blowup behavior is stable for parameter combinations other than the ones used in the

numerical simulations reported here.

In summary, both the existence and the stability of two-pulse solutions depend crucially on the semistrong nature of the interaction.

5.4. Relation to literature on finite-time blowup. For both modified Gierer–Meinhardt equations (5.2) and (5.7), the associated ODEs that govern spatially homogeneous patterns have solutions with small initial conditions that grow arbitrarily large. Therefore, in a certain sense, the discovery of finite-time blowup for the PDEs is not a surprise. A more detailed examination of the mechanism(s) responsible here is under way and is beyond the scope of this article.

At first glance, for both (5.2) and (5.7), the spatially localized V profile acts as a source in the linear equation for U, and the amplitude of this source is $1/\varepsilon^2$, which is large compared to the $\mathcal{O}(1)$ decay rate (μ) of U. Hence unbounded growth in U is possible.

Now, for (5.7) with μ not too large, we observe the following interplay between the growth of U and V. The maximum value of V along the homoclinic orbit/pulse is given to leading order by $V_{\max} \sim 3/[2((1/U) + (\beta/\sqrt{U}))]$; see (2.7). Hence, as the (maximum) value of U at a pulse center increases, so does $V_{\max}$, which in turn fuels a further increase in U since V acts as a source term in the U equation, etc. In this sense, there appears to be a positive feedback loop, with the growth in the components reinforcing each other.

In addition, for (5.7), as reported above, there is a transition from blowup in finite time to self-replication at sufficiently large μ. In other words, as μ increases, there appears to be a transition to a regime in which the decay rate μ is strong enough to balance the large source term and hence prevent unbounded growth.

For (5.2), the mechanism causing the finite-time blowup appears to be different. In fact, as suggested by [46], the mechanism here may be similar to the known (see below) blowup results for self-similar solutions of scalar reaction-diffusion equations of the form $V_t = DV_{xx} - V + V^2$. More precisely, $g(U) \to \alpha$, a constant, as U gets large. Hence the V equation essentially decouples (for large U) and is of this classical form.

The literature on finite-time blowup in reaction-diffusion equations and systems is large. We cite three interesting examples of coupled reaction-diffusion equations in which the reactions are given by polynomials and in which blowup in finite time is known to occur. First, [37] establishes the blowup of the catalyst concentration b in the isothermal autocatalytic reaction $A \to B$ that has rate constant kab^n with $n \geq 1$ (i.e., in so-called nth order autocatalysis). In the limit that the ratio of the activator diffusivity to the inhibitor diffusivity is asymptotically small, it is shown that blowup occurs at a point in infinite time for $n \in [1, 2]$ and in finite time for $n > 2$. Second, [29] demonstrates the blowup of solutions of the coupled system $u_t = d_1\Delta u + u(a_1 - b_1u + c_1v)$, $v_t = d_2\Delta v + v(a_2 + b_2u - c_2v)$ with homogeneous Neumann boundary conditions and where the b_i, c_i, and d_i are all positive, where the a_i are real numbers, and where Δ denotes the Laplacian on R^N. Third, [17] presents "Fujita-type" blowup and global existence results for systems $u_t = \Delta u + u^{p_1}v^{q_1}$, $v_t = \Delta v + u^{p_2}v^{q_2}$, where the powers satisfy certain inequalities.

This third work, among others, extends the classical results of [20] for the scalar equations $u_t = \Delta u + f(u)$, where $f(u) > 0$ for $u > 0$. Fujita proved the existence of nonnegative solutions that decay sufficiently rapidly at infinity and that blow up in finite time for $f(u) = u^p$ with

$1 < p < 1 + (2/N)$, and he showed that, for p larger than critical, all solutions generated from small initial data exist for all time [20]. Hence one may say (see also [27]) that, in the former case, small data grows due to the reaction term and the diffusion is not strong enough to stabilize it, whereas, in the latter case, the diffusion is strong enough to prevent unbounded growth. Also, we refer to [19] for a seminal analysis of blowup in this equation on bounded domains and to the useful article [27] that reviews and presents various extensions of the classical results.

For completeness, we also mention that it has already been shown that diffusion can destabilize a globally stable equilibrium of the reaction kinetics in such a strong manner that there is blowup in finite time for certain pairs of weakly coupled systems. See [49] and the references there. Also, [41] presents new results showing that blowup in the L^∞ norm is possible for solutions of pairs of reaction-diffusion equations with mass dissipation even if there is an a priori bound on the solution in the L^1 norm. However, neither of our modified Gierer–Meinhardt models satisfies the hypotheses made in these works.

6. Attracting and repelling stationary two-pulse solutions. In this section, we study systems of the form (1.1) that satisfy the following:

(i) The function $g'(u)$ has one simple zero, say, at $u = \alpha$ (which differs from the α used in section 5.2).

(ii) The function $H(u)$ again has one simple zero.

Condition (ii) is the same as that imposed in section 4, where we recall that, geometrically, it implies that ℓ^u and $T_o(0)$ intersect transversely at a unique point (and similarly for ℓ^s and $T_d(0)$). However, condition (i) is different, and the presence of the zero of $g'(u)$ dramatically alters the locations of the takeoff and touchdown curves $T_o(\hat{c}_i)$ and $T_d(\hat{c}_i)$, $i = 1, 2$, respectively, and makes possible a richer pulse dynamics, as we will see below.

We assume, for ease of presentation, that the condition (4.3) holds, and we consider the following three cases:

$$\begin{aligned} &\text{Case I:} && 0 < \alpha < \pi_u(\ell^u \cap T_o(0)), \\ &\text{Case II:} && \pi_u(\ell^u \cap T_o(0)) < \alpha < \pi_u(\mathcal{F}(\ell^u) \cap \mathcal{F}^{-1}(\ell^s)), \\ &\text{Case III:} && \pi_u(\mathcal{F}(\ell^u) \cap \mathcal{F}^{-1}(\ell^s)) < \alpha, \end{aligned} \tag{6.1}$$

where we recall that π_u denotes the projection onto the u-coordinate. These three cases include all of the structurally different cases, so we see that the assumption (4.3) is not restrictive.

In all three cases, we consider symmetric singular two-pulse solutions (symmetric about $x_0 = 0$). These are constructed exactly as the two-pulse solutions in section 4 were constructed. Their left and right pulses have slow and fast segments that are defined in terms of the intersection points O_1, D_1, O_2, and D_2, although the locations of these points differ because the positions of the curves $T_o(\hat{c}_i)$, $T_d(\hat{c}_i)$, $\mathcal{F}(\ell^u)$, and $\mathcal{F}^{-1}(\ell^s)$ are different. Moreover, there are two sets of such points in case II, which is the feature that makes the richer pulse dynamics possible. See Figure 6.1.

The main outcome of the analysis in this section is that a pair of slowly varying two-pulse solutions does not necessarily reach either the weak interaction limit ($\Delta\Gamma \to \infty$) or the strong interaction limit ($\Delta\Gamma \downarrow 0$). Slowly varying two-pulse solutions may also converge to a stationary two-pulse solution of the semistrong type. We present the essence of the analysis

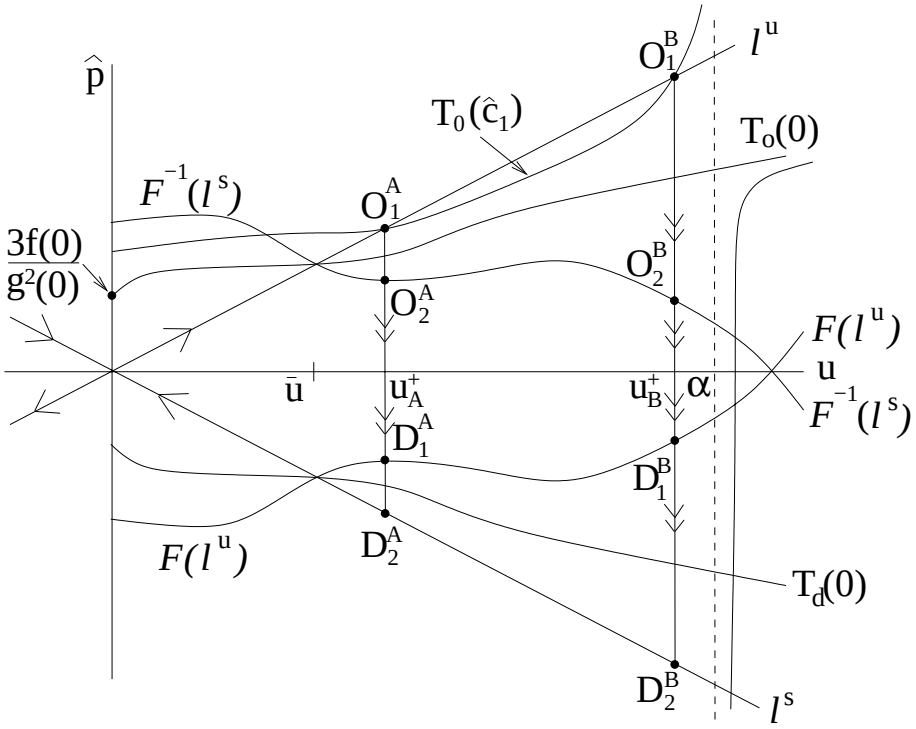

Figure 6.1. *The geometry of the curves $T_o(0)$, $T_o(\hat{c}_1)$, $T_d(0)$, ℓ^u, ℓ^s, $\mathcal{F}(\ell^u)$, and $\mathcal{F}^{-1}(\ell^s)$, along with their intersections, on the invariant manifold $\mathcal{M}$ for case* II *in the case studied in section* 6.1. *The curve $T_d(\hat{c}_2)$ is not shown in order not to clutter the figure. There are two sets of takeoff and touchdown points O_1^A, D_1^A, O_2^A, and D_2^A as well as O_1^B, D_1^B, O_2^B, and D_2^B, as shown in section* 6.1, *and hence two different singular, slowly varying, two-pulse solutions. The intersection $\mathcal{F}(\ell^u) \cap \mathcal{F}^{-1}(\ell^s)$ occurs at a point on the u-axis, denoted $\pi_u(\mathcal{F}(\ell^u) \cap \mathcal{F}^{-1}(\ell^s))$ in the text. Also, $\bar{u} = \pi_u(\ell^u \cap T_o(0))$.*

for the most general case since the details are similar to those in section 4. We do, however, give the details in the context of a specific example.

Remark 6.1. Throughout this section, we will assume, for the sake of definiteness, that $g'' < 0$ at $u = \alpha$. This implies that $g'(u) > 0$ for $u < \alpha$ and $g'(u) < 0$ for $u > \alpha$. The results for the opposite situation can be obtained in the same manner.

6.1. Case II. In case II, there exist two types of symmetric, slowly varying, two-pulse solutions. Moreover, there also exists a symmetric, stationary, two-pulse solution that attracts the slowly varying solutions for $g''(\alpha) < 0$ and repels them for $g''(\alpha) > 0$. We construct these slowly varying solutions and determine ODEs for the pulse separation distances.

Following the blueprint of section 3, we begin with the curves $T_o(\hat{c}_1)$, $T_d(\hat{c}_1)$, ℓ^u, ℓ^s, $\mathcal{F}(\ell^u)$, and $\mathcal{F}^{-1}(\ell^s)$. Recall from (2.18) that $T_o(\hat{c}_1)$ and $T_d(\hat{c}_1)$ are given by

$$\hat{p} = 2\hat{c}_1 \frac{g(u)}{g'(u)} \pm \frac{3f(u)}{g^2(u)}.$$

Hence, for $\hat{c}_1 > 0$, $T_o(\hat{c}_1)$ lies above $T_o(0)$ on $u < \alpha$, whereas it lies below $T_o(0)$ on $u > \alpha$

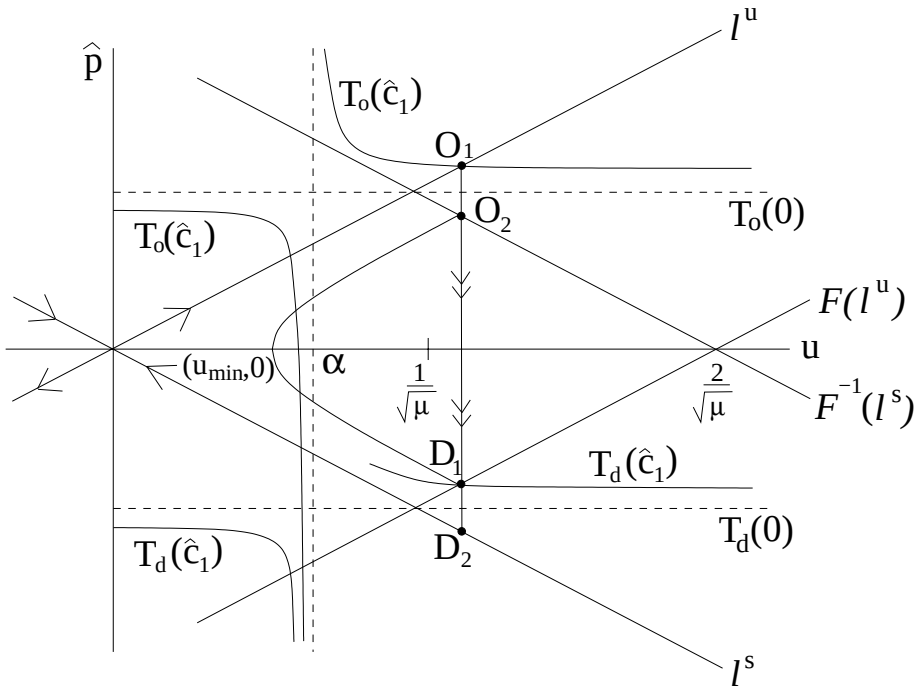

Figure 6.2. *The geometry on the invariant manifold $\mathcal{M}$ for case* I *studied in section* 6.2. *For definiteness, we have based some elements of the sketch on properties of the example in section* 6.3.

because of the assumptions (4.3) and $g''(\alpha) < 0$. Similarly, $T_d(\hat{c}_1)$ lies above $T_d(0)$ on $u < \alpha$ and below it on $u > \alpha$; see Figure 6.1. Moreover, these results would be reversed if one instead had $\hat{c}_1 < 0$.

We observe that, since the intersection $\ell^u \cap T_o(0)$ consists of a single point by assumption (ii), the curve $\mathcal{F}^{-1}(\ell^s)$ must intersect these two curves also at the same point. Similarly, ℓ^s, $T_d(0)$, and $\mathcal{F}(\ell^u)$ intersect in a point, symmetrically disposed about the u-axis with respect to the intersection point $\ell^u \cap T_o(0) \cap \mathcal{F}^{-1}(\ell^s)$; see Figures 6.1 and 6.2.

As illustrated in Figure 6.1, the geometry of these curves is such that, for an interval of positive $\hat{c}_1$ values, the intersection $T_o(\hat{c}_1) \cap \ell^u$ consists of at least two points. There could be others in between. That there exist at least two follows from the fact that $T_o(\hat{c}_1)$ can be taken to be close to $T_o(0)$ over as large a portion of the interval $(0, \alpha)$ as one pleases by choosing $\hat{c}_1$ small enough. Hence the first intersection point, labeled O_1^A, exists and lies close to the intersection point of ℓ^u and $T_o(0)$ for small $\hat{c}_1$. We denote its u-coordinate by u_A^+. The existence of the second intersection point, labeled O_1^B, then follows directly from the observation that, for each $\hat{c}_1$, $T_o(\hat{c}_1)$ has a vertical asymptote at $u = \alpha$ since $g'(u)$ has a simple zero there. The u-coordinate of O_1^B, which we label u_B^+, lies close to α for $\hat{c}_1$ small. Finally, there is a maximum value of $\hat{c}_1$ such that, at the maximum, $T_o(\hat{c}_1)$ has only a tangency to ℓ^u and, for values of $\hat{c}_1$ larger than the maximum, $T_o(\hat{c}_1)$ no longer intersects ℓ^u.

The singular solution for the A-pulse consists of the following segments:

- left slow on $(-\infty, \Gamma_1(t))$: $(0,0)$ to O_1^A along ℓ^u;

- left fast at $x = \Gamma_1(t)$: O_1^A to D_1^A;
- middle slow on $(\Gamma_1(t), 0] \cup [0, \Gamma_2(t))$: $D_1^A \to (u_{\min}, 0) \to O_2^A$;
- right fast at $x = \Gamma_2(t)$: O_2^A to D_2^A;
- right slow on $(\Gamma_2(t), \infty)$: D_2^A to $(0,0)$ along ℓ^s.

The singular B-pulse is the same type of solution, except with the superscripts A replaced by B.

Next, we turn to the ODE for the pulse separation distance $\Delta\Gamma(t) = \Gamma_2(t) - \Gamma_1(t)$. We recall from (4.11) that $\Delta\Gamma(t)$ satisfies

$$\frac{d}{dt}\Delta\Gamma = -3\varepsilon^3 \frac{f(u^+)g'(u^+)}{g^3(u^+)} e^{-\varepsilon\sqrt{\mu}\Delta\Gamma}. \tag{6.2}$$

This ODE has a unique, nontrivial, fixed point at $u^+ = \alpha$ for all values of α in case II because α is the unique zero of $g'(u)$ by assumption (i). This value of u^+ corresponds to a symmetric, stationary, two-pulse solution for which the pulse separation distance is

$$\Delta\Gamma_{\text{stat}} = \frac{-1}{\varepsilon\sqrt{\mu}} \ln\left(\sqrt{\mu}\mathcal{G}(\alpha) - 1\right), \tag{6.3}$$

which is a strictly $\mathcal{O}(1/\varepsilon)$ quantity; see the definition (4.13) of $\mathcal{G}$, and see also (4.12). This fixed point is a two-circuit homoclinic solution of the stationary problem associated to the PDE (1.1), i.e., of the ODE (2.3) with $\hat{c} = 0$; see also Remark 6.2 below. It corresponds to a stable fixed point of (6.2) because we have assumed that $g'(u) > 0$ on $u < \alpha$ (and to an unstable point in the opposite case).

For the A-pulse, the ODE (6.2) with $u^+ = u_A^+$ governs the pulse separation distance, and for the B-pulse, the ODE is also (6.2) but with $u^+ = u_B^+$. Both solutions are attracted to the symmetric, homoclinic, two-pulse fixed point. However, the A- and B-type pulses are not necessarily different for all time: during the evolution, a pair of A-pulses may change into a pair of B-pulses. In other words, a pair of slowly varying pulses might start as being of type A, and then, after a certain time, when $\Delta\Gamma$ has decreased below a critical value or, equivalently, when $|\hat{c}|$ has reached a certain maximal value, the pulses become of type B. See section 6.3 for an explicit example.

Remark 6.2. The existence of the symmetric, stationary, two-pulse solution does not follow directly from the results of sections 2 and 3. Nevertheless, these solutions can be rigorously constructed in all three cases. A crucial observation is that (2.12) does not directly imply (2.13) but a slightly different version, namely, $\hat{p}g'(u) = \hat{c}g(u)$. Thus the intersection of $W^U(\mathcal{M})$ and $W^S(\mathcal{M})$ occurs for $\hat{c} = 0$ either at $\hat{p} = 0$ or at $u = \alpha$. The new two-circuit homoclinic orbit can now be constructed using the new $u = \alpha$ branch of $W^U(\mathcal{M}) \cap W^S(\mathcal{M})$. These homoclinic orbits are truly pulses of semistrong type, with the U-component slowly varying in between the pulses. This contrasts with the multipulse homoclinic orbits constructed in [9] for the Gray–Scott problem and in [7] for the more general class of problems of the type (1.1), for which the pulses are so close together that the U-component remains constant to leading order between them.

6.2. Cases I and III: Repelling or attracting two-pulse solutions. In case I, there exists a stationary, homoclinic, two-pulse solution and one type of symmetric, slowly varying, two-pulse solution in which the pulses repel, i.e., $\hat{c}_1 < 0$ and $\hat{c}_2 = -\hat{c}_1 > 0$. For $\hat{c}_1 < 0$, $T_o(\hat{c}_1)$ lies

below $T_o(0)$ on $u < \alpha$ and above it on $u > \alpha$ due to the assumption that $g''(\alpha) < 0$. Similarly, $T_d(\hat{c}_1)$ lies below $T_d(0)$ on $u < \alpha$ and above it on $u > \alpha$. Moreover, much is known for small values of $\hat{c}_1$ about the locations of these curves relative to the curves $T_o(0)$ and $T_d(0)$, just as in case II above. The unique, singular, two-pulse solution in case I is of the same type as the singular solutions constructed in case II, and it is sketched in Figure 6.2. Finally, from the ODE (6.2), we see that the two slowly varying pulses repel each other since $\alpha < \pi_u(\ell^u \cap T_0(0))$ here and since $u^+ > \alpha$ implies $g'(u^+) < 0$ by the assumption made on $g''(\alpha)$ throughout this section. See Figure 6.2. Thus, although there is a stationary two-pulse solution and a slowly varying two-pulse solution, these solutions cannot approach each other as time evolves due to geometric obstructions.

Finally, in case III, singular, slowly varying, two-pulse solutions can be constructed along the same lines as in the above cases. The pulses attract when $g''(\alpha) < 0$, which is the assumption made throughout this section, and they repel in the opposite case when $g''(\alpha) > 0$. Moreover, in the attracting case, there is an α_{crit} such that, if $\alpha > \alpha_{\text{crit}}$, then the pulses accelerate toward each other, whereas, if $\alpha < \alpha_{\text{crit}}$, then the rate of approach decreases. For general systems, α_{crit} is determined by requiring that the tangency between ℓ^u and $T_o(\hat{c}_1)$ occurs on the boundary at $u = \pi_u(\mathcal{F}(\ell^u) \cap \mathcal{F}^{-1}(\ell^s))$. See also the example in section 6.3.

Remark 6.3. In case I, there are other intersection points $\ell^u \cap T_0(\hat{c}_1)$; however, these do not lead to singular, slowly varying, two-pulse solutions. For example, as shown in Figure 6.2 with $\hat{c}_1 < 0$, a fast jump that starts at a takeoff point $\ell^u \cap T_0(\hat{c}_1)$ to the left of $u = \alpha$ lands on $\mathcal{F}(\ell^u)$ at a point below ℓ^s. Hence, after it lands, the singular solution is brought to the negative $\hat{p}$-axis by the slow flow, and it is not possible to complete a singular two-pulse solution of the type we study. Other possible intersection points share the same type of difficulty.

6.3. A fourth example. We briefly illustrate the results of this section on problems (1.1) for which $g(U) = e^{\gamma(U)}$, with $\gamma'(U) = 2(\alpha - U)/\beta$ and $\alpha, \beta > 0$, and for which $f(U) = g^2(U)/3$. Hence we model a general function g for which $g'(u)$ has one simple zero (at α), but we restrict the choice of f for the purpose of illustration, as was also done in the example of section 5.1. This example exhibits some interesting dynamics and illustrates various characteristics of the dynamics in cases I–III.

The important curves on $\mathcal{M}$ are branches of hyperbolas and lines, respectively,

$$\begin{aligned} T_o(\hat{c}), T_d(\hat{c}) &: \qquad \hat{p} = \frac{\hat{c}\beta}{\alpha - u} \pm 1, \\ \mathcal{F}(\ell^u), \mathcal{F}^{-1}(\ell^s) &: \qquad \hat{p} = \pm\sqrt{\mu}u \mp 2, \end{aligned}$$

so that $\ell^u \cap T_0(0)$ occurs at $u = 1/\sqrt{\mu}$ and $\mathcal{F}(\ell^u) \cap \mathcal{F}^{-1}(\ell^s)$ occurs at $u = 2/\sqrt{\mu}$. Moreover, the ODE (6.2) becomes

$$\frac{d\Delta\Gamma}{dt} = \frac{-2\varepsilon^3}{\sqrt{\mu}\beta}[\alpha\sqrt{\mu} - 1 - e^{-\varepsilon\sqrt{\mu}\Delta\Gamma}]e^{-\varepsilon\sqrt{\mu}\Delta\Gamma}. \tag{6.4}$$

Note that the stationary, homoclinic, two-pulse solution corresponds to the fixed point of this ODE that is determined by $\Delta\Gamma_{\text{stat}} = (-1/\varepsilon\sqrt{\mu})\ln(\alpha\sqrt{\mu} - 1)$.

Case II corresponds to $\alpha \in (1/\sqrt{\mu}, 2/\sqrt{\mu})$. In this case, the pulses in a slowly varying two-pulse solution attract each other. The speed of attraction varies. From (4.5), we find

$$\frac{d^2}{dt^2}\Delta\Gamma = -2\varepsilon^3 \frac{d\hat{c}_1}{dt}.$$

Then differentiation of the ODE (6.4) yields

$$\frac{d\hat{c}_1}{dt} = \frac{\varepsilon}{\beta}[2e^{-\varepsilon\sqrt{\mu}\Delta\Gamma} - \alpha\sqrt{\mu} + 1]e^{\varepsilon\sqrt{\mu}\Delta\Gamma}\left(\frac{d}{dt}\Delta\Gamma\right). \tag{6.5}$$

Therefore, since $\frac{d}{dt}\Delta\Gamma < 0$ in case II and since $\beta > 0$ by assumption, there exists a critical separation distance,

$$\Delta\Gamma_\star = \frac{-1}{\varepsilon\sqrt{\mu}} \ln\left(\frac{1}{2}(\alpha\sqrt{\mu} - 1)\right), \tag{6.6}$$

such that $\frac{d}{dt}\hat{c}_1 = 0$ for $\Delta\Gamma = \Delta\Gamma_\star$. In addition, $\hat{c}_1(t)$ increases for $\Delta\Gamma > \Delta\Gamma_\star$, while $\hat{c}_1(t)$ decreases for $\Delta\Gamma_{\text{stat}} < \Delta\Gamma < \Delta\Gamma_\star$.

For the A-pulses, the pulses accelerate toward each other; i.e., $\hat{c}_1(t)$ increases, while, for the B-pulses, the rate of approach decreases in time. Moreover, there can be a dynamic change-over from type-A pulses to type-B pulses. This occurs, for example, with pulse pairs for which $\Delta\Gamma(0)$ exceeds $\Delta\Gamma_\star$. The pulses are first of the A type and accelerate toward each other. Then, when the separation distance has decreased to $\Delta\Gamma_\star$, the pulses change to being of type B, and their speeds decrease as the two-pulse solution approaches the stationary two-pulse solution.

In case III, the critical value of α at which the switch-over from deceleration to acceleration occurs is $\alpha_{\text{crit}} = 3/\sqrt{\mu}$. This may be determined as follows. We recall that $\mathcal{F}(\ell^u)$ and $\mathcal{F}^{-1}(\ell^s)$ intersect at $u = 2/\sqrt{\mu}$. Hence, by examining the intersection of $T_o(\hat{c})$ and ℓ^u at that u value, we find that the critical wave speed is

$$\hat{c}_{\text{crit}} = \frac{\alpha - \frac{2}{\sqrt{\mu}}}{\beta}.$$

Moreover, at this same value of u, the above intersection is a quadratic tangency, and hence, by equating the derivatives with respect to μ of the expressions for $T_o(\hat{c}_{\text{crit}})$ and ℓ^u, we find the above value of α_{crit}.

7. Discussion.

In this section, we discuss the stability of the pulse patterns and the validity of the asymptotic construction. Also, we discuss several extensions of the theory developed in this article, first to the larger class of systems (1.2) and then to a number of different types of N-pulse solutions for $N \geq 3$.

7.1. Stability and validity.

In this article, we considered the existence problem for interacting pulses; i.e., we have developed a method by which the dynamics of semistrong pulses can be described. We now briefly discuss their stability and the closely related issue of the validity of the asymptotic construction.

We begin with the stationary pulses and the pulses that are stationary in a comoving frame. A rigorous result on the existence of the homoclinic orbits associated to the intersections

$\ell^u \cap T_o(0)$ follows by geometric singular perturbation theory. It is a straightforward application of the methods developed in [7, 9]. (See also [8] for much more exotic singular patterns constructed by these methods.) Thus the validity of the asymptotic construction can be established also in this case. The validity of the more complex (stationary and traveling) multipulse patterns of sections 6 and 7, which are associated to zeros of g', can also be obtained along these lines (although here the procedure might be a little less straightforward; see also Remark 6.2).

In [5, 6, 7], a method has been developed by which the stability of stationary-pulse solutions of two-component, singularly perturbed, reaction-diffusion equations can be studied in full analytical detail. This method, the so-called nonlocal eigenvalue problem (NLEP) method, extends the Evans function approach of [1] to singularly perturbed systems of the same type as (1.1) and (1.2). A crucial ingredient of the NLEP method is the reduction of the eigenvalue problem, which is a coupled system of two second order equations, associated to the stability of a pulse to a single, second order, inhomogeneous equation of Sturm–Liouville type that has a nonlocal term.

The NLEP method can be applied directly to the stability problem for a stationary, homoclinic, one-pulse solution $(U_h(\xi), V_h(\xi))$ of (1.1). We give a brief sketch of the procedure and refer to [6, 7] for the details. In order to study the spectral stability of $(U_h(\xi), V_h(\xi))$, we set

$$(U(x,t), V(x,t)) = (U_h(\xi) + u(\xi)e^{\lambda t}, V_h(\xi) + v(\xi)e^{\lambda t}),$$

substitute this into (1.1), and linearize. As stated above, the coupled second order equations for u and v are then reduced to the corresponding NLEP problem,

$$(\mathcal{L}(\xi) - \lambda)v \equiv v_{\xi\xi} + [2g(U_h)V_h - (1+\lambda)]v = -V_h^2 g'(U_h) \tag{7.1}$$

with $v(\xi)$ and λ such that

$$t_2(\lambda) = 1 - \frac{1}{2\sqrt{\mu+\lambda}} \int_{-\infty}^{\infty} [f'(U_h)V_h^2 + 2f(U_h)V_h v] d\xi = 0. \tag{7.2}$$

Here, the expression for t_2 arises from an analysis of the u equation in both the fast and the slow limits. The function $t_2(\lambda)$ is the so-called slow transmission function; it is a factor in the Evans function $\mathcal{D}$ associated to the stability problem [6, 7].

For almost all λ (see [6, 7]), there exist bounded solutions to (7.1), and then the eigenvalues are selected by applying the additional constraint (7.2). So, it is convenient to express the system—equation plus constraint—as a single, nonlocal equation,

$$w_{\xi\xi} + [2g(U_h)V_h - (1+\lambda)]w = 2V_h^2 g'(U_h) \frac{\int_{-\infty}^{\infty} f(U_h)V_h w d\xi}{\int_{-\infty}^{\infty} f'(U_h)V_h^2 d\xi - 2\sqrt{\mu+\lambda}} \tag{7.3}$$

[5, 6, 7]. We briefly consider the NLEP (7.1), (7.3) here to indicate that the sign of g' plays a significant role in the stability analysis. The full stability problem is in itself the subject of an independent investigation.

First, (7.1) strongly suggests that the two- (and N-) pulse solutions that can be constructed when g' has zeros—see section 6—can be expected to be unstable. It follows from the character

of the pulse solutions that the homogeneous Sturm–Liouville problem $\mathcal{L}v = \lambda v$ associated to (7.1) must have an unstable eigenvalue $\lambda_0^{\text{fast}} > 0$ [7]. In general, this eigenvalue can be stabilized by the coupling of (7.1) to the slow nonlocal equation (7.2) [6, 7]. However, this coupling does not exist when $g'(U_h) = 0$, which is the case for the stationary two-pulse solutions. Thus it is to be expected that λ_0^{fast} is (to leading order) also an unstable eigenvalue of the full problem. Of course, this statement is far from rigorous; it is a fully heuristic argument that neglects several possible additional stabilizing effects. Nevertheless, the argument shows that the existence and stability analysis are intertwined, a feature that is common in the analysis of localized solutions.

Second, a preliminary analysis of (7.1) and (7.2) indicates that there is a regime in parameter space in which there are stable homoclinic pulses when $g' < 0$ (i.e., in the case in which the two-pulse solutions consist of repelling pulses). Here, the underlying mechanism is more subtle. The above-mentioned unstable eigenvalue λ_0^{fast} corresponds to an eigenvalue $\lambda_0(\mu)$ of the full equation in the sense that $\lim_{\mu\to 0} \lambda_0(\mu) = \lambda_0^{\text{fast}}$ [7]. In the Gray–Scott model studied in [6] and in the generalized Gierer–Meinhart equations studied in [7], this eigenvalue merges, as μ increases, with a second positive eigenvalue $\lambda_1(\mu)$ to form a complex conjugate pair of eigenvalues. This pair crosses the imaginary axis in the λ plane at a critical Hopf-bifurcation value of μ that stabilizes the pulse.

On the contrary, this same preliminary analysis suggests that the homoclinic pulses in systems for which $g' > 0$—i.e., in the case of attracting two-pulse solutions—will be unstable in general. The above-mentioned second positive eigenvalue $\lambda_1(\mu)$ cannot exist when $g' > 0$. Hence the pulse cannot be stabilized (at least not by the mechanism studied in [6, 7]).

It is clear that, on the one hand, the stability problem is far from being solved and, on the other hand, that the methods of [5, 6, 7] are strong enough to be applied here. However, these methods are developed in the context of stationary pulses. The slowly varying pulses constructed in this article are not of that type. Therefore, one has to extend the methods of [5, 6, 7] in order to be able to consider the interacting pulses. This is the essential next step in the analysis of semistrong pulse interactions. A first (and formal) result in that direction has been obtained in [3, 4]. Using the ideas of [5, 6], it was possible to derive slowly varying eigenvalues that governed the short time stability of the slowly varying pulses in the Gray–Scott equation. Again, the situation differs in an important aspect from that of the weak interaction case since the eigenvalues will undergo $\mathcal{O}(1)$ changes during the time evolution of the system.

Preliminary analysis indicates—under some additional conditions—that repelling pulse pairs can be stable (through the same stability mechanism that stabilizes the homoclinic pulses). Furthermore, we note that, in each of the systems in which $g'(u) < 0$ that we have simulated numerically, the numerical simulations also suggest that repelling-type two-pulse solutions can be stable on the time scales on which they exist. However, as we have seen in the example of section 5.3, the changes in the eigenvalues might be able to trigger bifurcations/destabilizations that are not present in the stationary (or weak interaction) limit. In addition, since the homoclinic pulses are not likely to be stable for $g' > 0$, we do not expect stable pairs of attracting pulses.

Finally, we come to the question of the validity of the asymptotic construction of the slowly varying two-pulse solutions. As explained in section 3.2, we can still evoke the concepts

of geometrical singular perturbation theory to conclude that the singular pulses do persist. However, the nonrigorous part of the construction is not during the fast jumps but in the point of symmetry between the pulses where the solution to the left is "glued" to its symmetrical counterpart on the right. There, we describe the solutions by ODEs (2.3) that have different values of $\hat{c}$, so the connection cannot be smooth or, in other words, cannot be a solution of the PDE—see section 3.1. As explained in Remark 3.1, it can be shown that this problem can be solved in a consistent way at the higher order level—see also [4]—but such a consistent higher order expansion of course does not settle the validity of the construction.

In the case of weak interactions, the validity question is tackled either by a center manifold approach [12, 14] or by a renormalization approach [42]. Both methods exploit the fact that the associated homoclinic pulses are stable/attracting. These methods cannot be used directly in the semistrong case. However, it is likely that it is possible to use either of these approaches in a modified fashion to settle the validity in the semistrong case for the stable two-pulse solutions. To do so, one has to have full control on the (slowly varying) eigenvalues of these two-pulse solutions. Thus the validity issue is closely intertwined with the stability question.

We conclude that the stability and validity analysis of the pulse solutions constructed in this article is a significant problem. It is the subject of work in progress.

Remark 7.1. There is an alternative approach to the stability analysis of stationary one-pulse solutions of a certain, slightly more restrictive version of the Gierer–Meinhardt equation; see [23, 33, 48]. As in [5, 6, 7], the stability problem is reduced to a system of the same type as (7.3). However, the corresponding equation is of a different nature.

7.2. A more general class of PDEs. In the preceding sections, we focused on the class of PDEs (1.1) that includes many named models. However, examination of the techniques employed in sections 2, 3, 4, 5, and 6 reveals that they can also be applied to the much broader class of coupled reaction-diffusion equations (1.2), which, we recall, are

$$\left\{ \begin{array}{rcl} \varepsilon^{2+\sigma} U_t &=& U_{xx} + \varepsilon^2 F_1(U) + V F_2(U,V), \\ V_t &=& \varepsilon^2 V_{xx} + G(U,V). \end{array} \right. \tag{7.4}$$

Here, $\sigma \geq 0$, $0 < \varepsilon \ll 1$, and the functions F_1, F_2, and G are smooth for $U > 0$ and $V \geq 0$ and admit at most poles at $U = 0$. They also satisfy additional assumptions. We assume that $(U_0, V_0) = (0,0)$ is a linearly stable, homogeneous steady state of (1.2) and use the stretched variable $\xi = \frac{x - \Gamma(t)}{\varepsilon}$ in the comoving frame. Finally, we assume that the traveling wave ODE has a normally hyperbolic invariant manifold $\mathcal{M}$ for $\varepsilon = 0$ and that, on the persistent slow manifold, which may coincide with the $\varepsilon = 0$ manifold as for systems (1.1) or which may be $\mathcal{O}(\varepsilon)$ close to the plane $\{V = 0, V_\xi = 0\}$, the flow is superslow, i.e., slow in the slow/outer comoving variable $x - \Gamma(t)$.

The first generalization is to systems of the form (1.2) for which $F_1(U) = -\mu U$, $F_2(U,V) = h_1 U^{\alpha_1} V^{\beta_1}$, and $G(U,V) = -V + h_2 U^{\alpha_2} V^{\beta_2}$ with $\mu > 0$, $h_1 > 0$, and $h_2 > 0$, namely, to

$$\begin{array}{rcl} \varepsilon^2 U_t &=& U_{xx} - \varepsilon^2 \mu U + h_1 U^{\alpha_1} V^{\beta_1}, \\ V_t &=& \varepsilon^2 V_{xx} - V + h_2 U^{\alpha_2} V^{\beta_2}. \end{array} \tag{7.5}$$

We require that $\alpha_1 > 1 + \frac{\alpha_2 \beta_1}{\beta_2 - 1}$, $\alpha_2 < 0$, $\beta_1 > 1$, and $\beta_2 > 1$. This class of equations includes the generalized Gierer–Meinhardt equations; see [7, 21, 23, 33]. In [7], we showed the existence

and analyzed the stability of stationary, homoclinic, one-pulse solutions for systems (7.5) and also of multipulse homoclinic solutions consisting of a finite number of rapid pulses in quick succession; see Remark 6.2. In addition, in [8] we established the existence of stationary spatially periodic solutions, which are known to be attractors in the self-replication region, and we showed that on a sufficiently large interval one can construct a solution for any arbitrary prespecified pulse sequence.

While the flow on $\mathcal{M}$ is still linear due to the choice of F_1, the functions F_2 and G are more general than those in (1.1). The function $G = -V + h_2 U^{\alpha_2} V^{\beta_2}$ is a more general choice for which the reduced fast system,

$$0 = v_{\xi\xi} + G(\bar{u}, v), \tag{7.6}$$

has a homoclinic orbit to the saddle point $(0,0)$, and the choice of F_2 reflects the competing goals of wanting to have the most general possible form for F_2 but at the same time retain the necessary property that the fast jump, Δp, bridges the correct takeoff and touchdown points on $\mathcal{M}$.

Two-pulse solutions of the different types constructed in sections 3, 4, 5, and 6 (and N-pulse solutions of the types studied below in section 7.3) can be constructed for systems (7.5) satisfying the above conditions following the same technique used above. Moreover, the system (7.5) is itself a normal form in the study of large-amplitude pulse solutions in coupled reaction-diffusion equations. See (1.1) and (1.2) in [7], and we refer the reader to the introduction and the appendix there for further details.

There is also a second level of generalization that we can make, and we conclude this section by briefly sketching the necessary ingredients. First we consider how general the choice of the function G can be. In particular, we look at all possible G for which the reduced fast system (7.6) supports a homoclinic orbit to the saddle fixed point $(v = 0, v_\xi = 0)$. Let $\bar{U}$ denote the value of the component U at the center of the pulse. This entails assuming that, for every $\bar{U} > 0$, $G(\bar{U}, 0) = 0$, $(\partial G/\partial V)(\bar{U}, 0) < 0$, $G(\bar{U}, V_1) = 0$ for some $V_1 > 0$, $(\partial G/\partial V)(\bar{U}, V_1) > 0$, and $G(\bar{U}, V) < 0$ for all $V \in (0, V_1)$. Second, we observe that there is a wide class of functions F_1 to which one can extend the results of this article. The leading order flow on the persistent slow manifold is given by

$$u_{xx} + \varepsilon^2 F_1(u) = 0, \tag{7.7}$$

which is automatically superslow. So, now, instead of choosing F_1 to be a linear function, as was done for both (1.1) and (7.5), it can be chosen to be any (nonlinear) function for which the fixed point of (7.7), which corresponds to the asymptotic state of the pulses, is a saddle fixed point, and for which the various takeoff and touchdown points on the persistent slow manifold can be connected via the jump, Δp determined by F_2, in the fast field. The requirement that the critical point $u, u_x = 0$, on the slow manifold is of saddle type is directly related to the (natural) assumption that the trivial background state $(U, V) \equiv (0, 0)$ is stable as a solution of the PDE (7.4). Examples of such nonlinear slow systems include planar Hamiltonian systems, such as the classical pendulum, the Duffing equation, and escape oscillators.

Remark 7.2. For the problem of resonance bands in Hamiltonian systems, one-pulse and multipulse (with alternating fast-slow segments) homoclinic orbits have been constructed in

[25]. There, the slow flow was given to leading order by the nonlinear pendulum with constant torque, adiabatic Melnikov theory was used to calculate the fast jumps, and geometric singular perturbation theory was used to assemble (and rigorously prove the existence of) the homoclinic orbits.

7.3. Beyond symmetric two-pulse solutions. In this last section, we give some straightforward extensions of the two-pulse results of the previous sections to establish the existence of stationary N-pulse solutions, traveling N-pulse solutions, and slowly varying N-pulse solutions for $N > 2$. These solutions are biasymptotic to $(U = 0, V = 0)$, just as was the case for $N = 2$, and they consist of N localized (fast) pulses in alternation with $N + 1$ slow segments. We sketch only the geometrical backbones of the constructions.

In order to construct some stationary N-pulse solutions, we focus on those PDEs (1.1) for which $g'(U)$ has one simple zero, again at $U = \alpha$, and for which $T_o(0)$ and ℓ^u intersect transversely in one point. Extensions to problems in which $g'(U)$ has more than one simple zero and/or in which $T_o(0)$ and ℓ^u intersect transversely in more than one point follow readily.

Singular, stationary, N-pulse solutions consist of the following segments, where $\hat{c} \equiv 0$ in the governing ODEs:

- left slow segment along ℓ^u from $(0, 0)$ to the takeoff point $O_1 \equiv \ell^u \cap \{u = \alpha\}$;
- left fast pulse from O_1 to the touchdown point $D_1 \equiv \mathcal{F}(\ell^u) \cap \{u = \alpha\}$;
- second slow segment along hyperbolic cosine orbit segment γ on $\mathcal{M}$ from D_1 to $O_2 \equiv \gamma \cap T_o(0)$;
- second fast pulse from O_2 to $D_2 \equiv \gamma \cap T_d(0)$;
- third through $(N-1)$th slow segments along γ from D_2 back to O_2, interspersed with the third through $(N-1)$th fast pulses, each of which connects O_2 to D_2;
- Nth slow segment along γ from D_2 to $O_N \equiv \mathcal{F}^{-1}(\ell^s) \cap \{u = \alpha\}$;
- Nth fast pulse from O_N to $D_N \equiv \ell^s \cap \{u = \alpha\}$;
- $(N+1)$th slow segment along ℓ^s from D_N to $(0, 0)$.

See Figure 7.1(a) for an illustration with $N = 5$. Moreover, the same type of geometric singular perturbation theory arguments (see also Remark 6.2) can be used here to show that there exists a true N-pulse solution for $0 < \varepsilon \ll 1$ near a singular ($\varepsilon = 0$) solution of the type just constructed. If we assume that (4.3) holds and that $\alpha > \pi_u(\ell^u \cap T_0(0))$, then the maximum values of u are highest at the tops of pulses $2, \ldots, N-1$ and slightly lower at the maxima of the first and Nth pulses; see Figure 7.1(a). Moreover, for each pulse in an N-pulse solution, the maximum of U exceeds that of the $(N = 1)$-pulse solution.

Next, we show how to construct N-pulse solutions that travel with constant wave speed, $\hat{c}(t) \equiv \hat{c}_N$. We do this for PDEs of the form (1.1) for which $g'(U)$ has one simple zero (again, at $U = \alpha$) but now for which $T_o(\hat{c}_1)$ and ℓ^u intersect transversely in at least two distinct points, one with U-coordinate less than α and the other with U-coordinate greater than α; see Figure 7.1(b). Here also, extensions are possible.

The ODE governing N-pulse classical traveling waves is (2.3) with $\hat{c}(t) \equiv \hat{c}_N$. We describe the singular solution for a traveling N-pulse solution with $N = 2$, which consists of the following segments:

- left slow segment along ℓ^u from $(0, 0)$ to the first takeoff point $O_1 \equiv \ell^u \cap T_0(\hat{c}_N)$, where $\pi_u(O_1) < \alpha$;

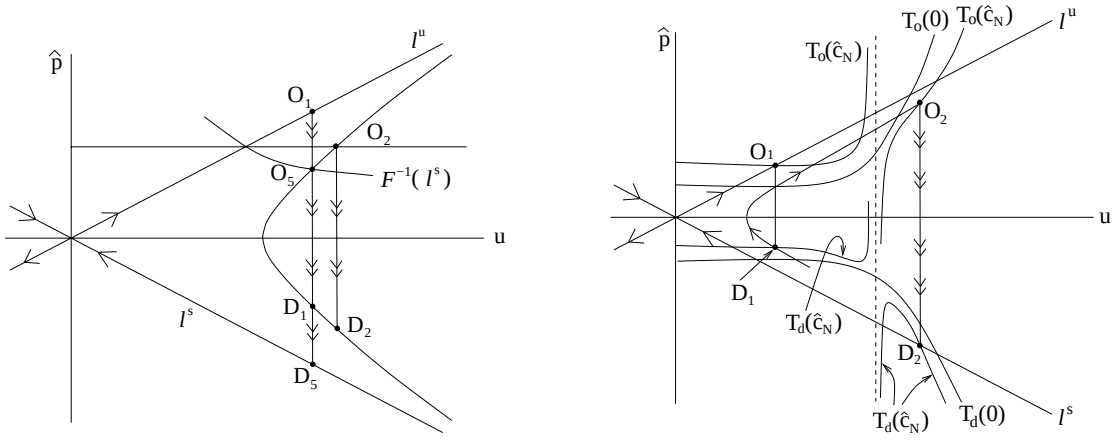

Figure 7.1. (a) *Sketch of a singular, stationary, N-pulse solution, with $N = 5$. The points O_3 and O_4 coincide with O_2, and the points D_3 and D_4 coincide with D_2.* (b) *Sketch of a singular, traveling, N-pulse solution, with $N = 2$.*

- left fast pulse from O_1 to the touchdown point $D_1 \equiv T_d(\hat{c}_N) \cap \{u = \pi_u(O_1)\}$;
- middle slow segment along a hyperbolic cosine orbit segment γ on $\mathcal{M}$ from D_1 to $O_2 \equiv \gamma \cap T_o(\hat{c}_N)$, where $\pi_u(O_2) > \alpha$;
- second fast pulse from O_2 to $D_2 \equiv \ell^s \cap T_d(\hat{c}_N)$;
- right slow segment along ℓ^s from D_2 back to $(0, 0)$.

See Figure 7.1(b). The generalization to $N > 2$ follows the same procedure. The wave speed $\hat{c}_N$ is selected by the relative positions of the various intersection points. (A small change in $\hat{c}_2$ in the construction in Figure 7.1(b) will remove the final touchdown point D_2 from ℓ^s.) Moreover, due to symmetries, if there exists a traveling N-pulse solution with wave speed $\hat{c}_N$, then there also exists a symmetrically disposed N-pulse traveling wave with speed $-\hat{c}_N$. Note that there are of course several conditions like (4.1) that have to be satisfied in order to be able to construct (stationary or traveling) multipulse solutions in the general PDE (1.1).

Finally, one can construct slowly varying N-pulse solutions by mimicking the results of section 4. For these solutions, the outermost pulses, i.e., the first and Nth pulses, move away from each other when $g'(U) < 0$ for all $u > 0$, and they move toward each other when $g'(U) > 0$ for all $u > 0$. Such an analysis would also be useful to further answer the questions of whether pulse-splittings are of the type 2^n or of the type for which just the edge pulses split. See [15] for the analysis of this question in the context of weak interactions.

Appendix. Coupled reaction-diffusion equations in general form. In this appendix, we briefly examine a number of named systems of coupled reaction-diffusion equations. We rescale the equations into a natural form associated to the singular character of the pulse solutions exhibited by these systems. We find that these natural forms are given by (1.1) or (1.2). Thus the methods developed in this article can be applied directly to any of these equations. Specifically, we examine the (classical and generalized) Gierer–Meinhardt equations, the Gray–Scott model, the Schnakenberg system, and the Thomas equations. The scaling analysis needed for the first two of these models has been derived earlier in [3, 4, 7, 10].

We begin with the classical Gierer–Meinhardt equations,

$$\begin{aligned} U_t &= U_{xx} - \mu U + V^2, \\ V_t &= DV_{xx} - V + \frac{V^2}{U}, \end{aligned} \tag{A.1}$$

where $\mu > 0$ and D is the ratio of the diffusivities, taken to be less than one following the usual Turing analysis. The scalings appropriate for large-amplitude pulse solutions are shown in [7, 10] to be

$$U = \frac{1}{\sqrt{D}}\hat{U}, \qquad V = \frac{1}{\sqrt{D}}\hat{V}, \qquad x = D^{1/4}\hat{x}.$$

Note that these scalings represent the fact that the amplitudes of both the U- and the V-components of the pulse solutions of (A.1) are $\mathcal{O}(1/\sqrt{D})$. The amplitudes of $\hat{U}$ and $\hat{V}$ will be $\mathcal{O}(1)$ in the natural scaled form (that will be of type (1.1)).

In terms of these scaled variables, the PDE (A.1) becomes

$$\begin{aligned} \sqrt{D}\hat{U}_t &= \hat{U}_{\hat{x}\hat{x}} - \mu\sqrt{D}\hat{U} + \hat{V}^2, \\ \hat{V}_t &= \sqrt{D}\hat{V}_{\hat{x}\hat{x}} - \hat{V} + \frac{\hat{V}^2}{\hat{U}}. \end{aligned}$$

Hence it is natural to introduce the parameter ε via

$$\varepsilon^2 = \sqrt{D}.$$

The scaled Gierer–Meinhardt equations therefore may be written in the normal form of the type (1.1), namely, as

$$\begin{aligned} \varepsilon^2\hat{U}_t &= \hat{U}_{\hat{x}\hat{x}} - \varepsilon^2\mu\hat{U} + \hat{V}^2, \\ \hat{V}_t &= \varepsilon^2\hat{V}_{\hat{x}\hat{x}} - \hat{V} + \frac{\hat{V}^2}{\hat{U}}. \end{aligned}$$

It was shown in [7] that stationary singular pulses exist for $\varepsilon^2 = \sqrt{D} \ll 1$ and that there is a Hopf bifurcation at μ_{Hopf} (≈ 0.36 to leading order) in the regime $\mu = \mathcal{O}(1)$ such that the pulses are stable for $\mu > \mu_{\text{Hopf}}$ and unstable for $\mu < \mu_{\text{Hopf}}$. In addition, it was shown in [10] that pulse splitting occurs in the regime in which $\mu = \mathcal{O}(1/\varepsilon^4)$. Finally, we remark that a similar analysis can be done for the generalized Gierer–Meinhardt equations, as shown in [7], provided that the conditions on the powers stated in [7] are satisfied.

Next, we turn our attention to singular-pulse solutions in the Gray–Scott model,

$$\begin{aligned} U_t &= U_{xx} - UV^2 + A(1-U), \\ V_t &= DV_{xx} + UV^2 - BV, \end{aligned} \tag{A.2}$$

where $A, B, D > 0$. Then the scaling introduced in [3, 4] (see especially equation (1.3) in [4]) is

$$x = \sqrt{\frac{D}{B}}\xi, \qquad U = \frac{B\sqrt{B}\sqrt{D}}{\sqrt{A}}\hat{U}, \qquad V = \sqrt{\frac{A}{BD}}\hat{V}.$$

The scaling of x reflects the narrowness of the pulses, and hence ξ is the appropriate stretched variable with which to analyze the localized pulses. The scalings of U and V reflect their amplitudes.

Substituting these scalings into the system (A.2), we obtain

$$\frac{D}{B}\hat{U}_t = \hat{U}_{\xi\xi} - \frac{A}{B^2}\hat{U}\hat{V}^2 + \frac{A\sqrt{A}\sqrt{D}}{B^2\sqrt{B}}\left(1 - \frac{B\sqrt{B}\sqrt{D}}{\sqrt{A}}\hat{U}\right),$$
$$\frac{1}{B}\hat{V}_t = \hat{V}_{\xi\xi} + \hat{U}\hat{V}^2 - \hat{V}.$$

Now, in order to put this scaled Gray–Scott PDE into the form of the general systems (1.2) studied here, one needs to look at this system in terms of the long (or slow) spatial variable and a scaled time,

$$\hat{x} = \frac{\sqrt{A}}{B}\xi, \qquad \hat{t} = Bt.$$

Also, the natural parameter groups that emerge are

$$\varepsilon^2 = \frac{A}{B^2}, \qquad \delta = \sqrt{BD}.$$

Furthermore, we introduce the parameter σ by

$$D = \varepsilon^{4+\sigma}. \tag{A.3}$$

Hence the Gray–Scott model may be written as

$$\varepsilon^{2+\sigma}\hat{U}_{\hat{t}} = \hat{U}_{\hat{x}\hat{x}} - \varepsilon^2\left[\frac{\delta}{\varepsilon}\left(\frac{\delta}{\varepsilon}\hat{U} - 1\right)\right] - \hat{U}\hat{V}^2,$$
$$\hat{V}_{\hat{t}} = \varepsilon^2\hat{V}_{\hat{x}\hat{x}} - \hat{V} + \hat{U}\hat{V}^2,$$

which is of the form of (1.1) modulo a simple linear shift in U if $\delta/\varepsilon = \mathcal{O}(1)$ and $\sigma = 0$, i.e., $D = \mathcal{O}(\varepsilon^4) = \mathcal{O}(A^2/B^4)$; recall (A.3). These conditions on the parameter play central roles in the analysis of the Gray–Scott equation [3, 4, 5, 9]. For instance, $\sigma = 0$ marks the transition (by a Hopf bifurcation) from unstable pulse patterns ($\sigma < 0$) to stable pulse patterns ($\sigma > 0$); these patterns include periodic patterns [5] and slowly varying two-pulse solutions [3, 4]. Note that this also implies that the condition $B^4D \ll A^2$ or $\sigma > 0$, i.e., the case in which the scaled Gray–Scott model is of the form (1.2), is a natural condition on the parameters A, B, and D in the original, unscaled, Gray–Scott equation (A.2). We refer the reader to [3, 4] for a detailed analysis of the existence, bifurcation, splitting, and stability of two-pulse solutions of the Gray–Scott model for the different parameter combinations.

Third, we look at the Schnakenberg model,

$$U_t = U_{xx} + \gamma(b - UV^2),$$
$$V_t = DV_{xx} + \gamma(a - V + UV^2), \tag{A.4}$$

where $a, b, \gamma \geq 0$, and we set $\gamma = 1$ for convenience. The reaction kinetics are very similar to those of the Gray–Scott model, except that there is a feed term for the activator and there is

no linear decay term for the inhibitor concentration. (Analysis of the Gray–Scott model with an activator-feed term is presented in [22, 40], and the analysis of the slowly varying two-pulse solutions presented in [3, 4] can be extended to this case.) There is a homogeneous steady state at the point $(b/(a+b)^2, b+a)$. See section 6.4 of [32] for analysis of the phase plane. While more general results can be found for $a > 0$, we analyze the special case $a = 0$ here for expedience.

Setting $D = \varepsilon^2$, we scale the variables as

$$U = \varepsilon^{\alpha}\hat{U}, \qquad V = \varepsilon^{-\alpha}\hat{V}, \qquad x = \varepsilon^{\alpha}\xi,$$

with $\alpha > 0$, since the u-component is small at the pulse center, whereas the v-component diverges as $\varepsilon \to 0$. Restricting ourselves to the interval $\alpha \in [1/2, 1)$, we find that the model (A.4) may be written as an equation of the form (1.1), (1.2)

$$\begin{aligned} \hat{\varepsilon}^{2+\sigma}\hat{U}_t &= \hat{U}_{\xi\xi} + \hat{\varepsilon}^2\hat{b} - \hat{U}\hat{V}^2, \\ \hat{V}_t &= \hat{\varepsilon}^2\hat{V}_{\xi\xi} - \hat{V} + \hat{U}\hat{V}^2, \end{aligned}$$

where we have scaled $b = \varepsilon^{2-3\alpha}\hat{b}$ and introduced $\hat{\varepsilon} = \varepsilon^{(1-\alpha)}$ and $\sigma = 4\alpha - 2$.

Note, however, that there is a certain difference here. The plane $V = 0, V_\xi = 0$ is again invariant and normally hyperbolic, although now there are no fixed points on it. So, instead of looking for one-pulse solutions of the homoclinic type that are biasymptotic to an equilibrium on the plane, we look for spatially periodic solutions that consist of periodic arrays of localized near-homoclinic pulses interspersed with slow segments exponentially close to solutions of the slow system on the plane. This can be done using the same machinery developed in [5] and further employed in [30] to study the spatially periodic solutions that are the attractors in the pulse-splitting regime of the Gray–Scott model, and here such periodic solutions are found to exist for $\alpha \in [2/3, 1)$.

Finally, we observe that a similar type of scaling analysis can be carried out on the Thomas equations,

$$\begin{aligned} U_t &= U_{xx} + \gamma\left(\alpha(b-U) - H(U,V)\right), \\ V_t &= DV_{xx} + \gamma\left(a - V + H(U,V)\right), \end{aligned}$$

where $H(U,V) = \rho UV/(1+V+KV^2)$, and all parameters are nonnegative; see Chapter 5 of [32]. We do not go into the details.

Acknowledgment. The authors thank the referees for comments that helped improve the presentation.

REFERENCES

[1] J. Alexander, R. A. Gardner, and C. K. R. T. Jones, *A topological invariant arising in the stability of traveling waves*, J. Reine Angew. Math., 410 (1990), pp. 167–212.

[2] J. G. Blom and P. A. Zegeling, *Algorithm* 731: *A moving-grid interface for systems of one-dimensional time-dependent partial differential equations*, ACM Trans. Math. Software, 20 (1994), pp. 194–214.

[3] A. Doelman, W. Eckhaus, and T. J. Kaper, *Slowly modulated two-pulse solutions in the Gray–Scott model* I: *Asymptotic construction and stability*, SIAM J. Appl. Math., 61 (2000), pp. 1080–1102.

[4] A. Doelman, W. Eckhaus, and T. J. Kaper, *Slowly modulated two-pulse solutions in the Gray–Scott model* II: *Geometric theory, bifurcations, and splitting dynamics*, SIAM J. Appl. Math., 61 (2001), pp. 2036–2062.
[5] A. Doelman, R. A. Gardner, and T. J. Kaper, *Stability analysis of singular patterns in the* 1*-D Gray–Scott model: A matched asymptotics approach*, Phys. D, 122 (1998), pp. 1–36.
[6] A. Doelman, R. A. Gardner, and T. J. Kaper, *A stability index analysis of* 1*-D patterns of the Gray–Scott model*, Mem. Amer. Math. Soc., 155 (2002).
[7] A. Doelman, R. A. Gardner, and T. J. Kaper, *Large stable pulse solutions in reaction-diffusion equations*, Indiana Univ. Math. J., 50 (2001), pp. 443–507.
[8] A. Doelman, T. J. Kaper, and H. van der Ploeg, *Spatially periodic and aperiodic multi-pulse patterns in the one-dimensional Gierer-Meinhardt equations*, Methods Appl. Anal., 8 (2001), pp. 387–414.
[9] A. Doelman, T. J. Kaper, and P. Zegeling, *Pattern formation in the one-dimensional Gray-Scott model*, Nonlinearity, 10 (1997), pp. 523–563.
[10] A. Doelman and H. van der Ploeg, *Homoclinic stripe patterns*, SIAM J. Applied Dynamical Systems, 1 (2002), pp. 65–104.
[11] W. Eckhaus, *Asymptotic Analysis of Singular Perturbations*, North–Holland, Amsterdam, 1979.
[12] S. Ei, *The motion of weakly interacting pulses in reaction-diffusion systems*, J. Dynam. Differential Equations, 14 (2002), pp. 85–137.
[13] S. Ei, M. Mimura, and M. Nagayama, *Pulse-pulse interactions in reaction-diffusion systems*, Phys. D, 165 (2002), pp. 176–198.
[14] S. J. Ei, Y. Nishiura, and B. Sandstede, *Pulse-Interaction Approach to Self-Replicating Dynamics in Reaction-Diffusion Systems*, in preparation.
[15] S.-I. Ei, Y. Nishiura, and K.-I. Ueda, 2^n*-splitting or edge-splitting? A manner of splitting in dissipative systems*, Japan J. Indust. Appl. Math., 18 (2001), pp. 181–205.
[16] I. R. Epstein and J. A. Pojman, *An Introduction to Nonlinear Chemical Dynamics: Oscillations, Waves, Patterns, and Chaos*, Oxford University Press, Oxford, UK, 1998.
[17] M. Escobedo and H. A. Levine, *Critical blowup and global existence numbers for a weakly coupled system of reaction-diffusion equations*, Arch. Ration. Mech. Anal., 129 (1995), pp. 47–100.
[18] N. Fenichel, *Geometrical singular perturbation theory for ordinary differential equations*, J. Differential Equations, 31 (1979), pp. 53–98.
[19] A. Friedman and B. McLeod, *Blow-up of positive solutions of semilinear heat equations*, Indiana Univ. Math. J., 34 (1985), pp. 425–447.
[20] H. Fujita, *On the blowing up of solutions of the Cauchy problem* $u_t = \Delta u + u^{1+\alpha}$, J. Fac. Sci. Univ. Tokyo Sect. I, 13 (1966), pp. 109–124.
[21] A. Gierer and H. Meinhardt, *A theory of biological pattern formation*, Kybernetik, 12 (1972), pp. 30–39.
[22] P. Gray and S. K. Scott, *Autocatalytic reactions in the isothermal, continuous stirred tank reactor: Oscillations and instabilities in the system* $A + 2B \to 3B$, $B \to C$, Chem. Engrg. Sci., 39 (1984), pp. 1087–1097.
[23] D. Iron, M. J. Ward, and J. Wei, *The stability of spike solutions of the one-dimensional Gierer-Meinhardt model*, Phys. D, 150 (2000), pp. 25–62.
[24] C. K. R. T. Jones, *Geometric singular perturbation theory*, in Dynamical Systems (Montecatini Terme, 1994), Lecture Notes in Math. 1609, R. Johnson, ed., Springer-Verlag, Berlin, 1995, pp. 44–118.
[25] T. J. Kaper and G. Kovacic, *Multi-bump orbits homoclinic to resonance bands*, Trans. Amer. Math. Soc., 348 (1996), pp. 3835–3887.
[26] S. Kawaguchi and M. Mimura, *Collision of traveling waves in a reaction-diffusion system with global coupling effect*, SIAM J. Appl. Math., 59 (1999), pp. 920–941.
[27] H. A. Levine, *The role of critical exponents in blowup theorems*, SIAM Rev., 32 (1990), pp. 262–288.
[28] K.-J. Lin, W. D. McCormick, J. E. Pearson, and H. L. Swinney, *Experimental observation of self-replicating spots in a reaction-diffusion system*, Nature, 369 (1994), pp. 215–218.
[29] Y. Lou, T. Nagylaki, and W.-M. Ni, *On diffusion-induced blowups in a mutualistic model*, Nonlinear Anal., 45 (2001), pp. 329–342.
[30] D. S. Morgan, A. Doelman, and T. J. Kaper, *Stationary periodic orbits in the* 1*-D Gray-Scott model*, Methods Appl. Anal., 7 (2000), pp. 105–150.

[31] D. S. Morgan and T. J. Kaper, *Annular Rings and Their Destabilization into Spots in the* 2*-D Gray-Scott Model*, in preparation.
[32] J. D. Murray, *Mathematical Biology*, Biomathematics Texts 19, Springer-Verlag, Berlin, Heidelberg, New York, 1989.
[33] W.-M. Ni, *Diffusion, cross-diffusion, and their spike-layer steady states*, Notices Amer. Math. Soc., 45 (1998), pp. 9–18.
[34] Y. Nishiura and D. Ueyama, *A skeleton structure for self-replication dynamics*, Phys. D, 130 (1999), pp. 73–104.
[35] Y. Nishiura and D. Ueyama, *Spatio-temporal chaos for the Gray-Scott model*, Phys. D, 150 (2001), pp. 137–162.
[36] T. Ohta, *Pulse dynamics in a reaction-diffusion system*, Phys. D, 151 (2001), pp. 61–72.
[37] J. Olwoch and D. J. Needham, *Diffusion-driven blow-up in a reaction-diffusion model for* $n \geq 1$*-th order autocatalysis*, Nonlinearity, 13 (2000), pp. 43–76.
[38] M. Or-Guil, I. G. Kevrekidis, and M. Bär, *Stable bound states of pulses in an excitable medium*, Phys. D, 135 (2000), pp. 154–174.
[39] J. E. Pearson, *Complex patterns in a simple system*, Science, 261 (1993), pp. 189–192.
[40] V. Petrov, S. K. Scott, and K. Showalter, *Excitability, wave reflection, and wave splitting in a cubic autocatalysis reaction-diffusion system*, Phil. Trans. Roy. Soc. London Ser. A, 347 (1994), pp. 631–642.
[41] M. Pierre and D. Schmitt, *Blowup in reaction-diffusion systems with dissipation of mass*, SIAM J. Math. Anal., 28 (1997), pp. 259–269.
[42] K. Promislow, *A renormalization method for modulational stability of quasi-steady patterns in dispersive systems*, SIAM J. Math. Anal., 33 (2002), pp. 1455–1482.
[43] W. N. Reynolds, J. E. Pearson, and S. Ponce-Dawson, *Dynamics of self-replicating patterns in reaction diffusion systems*, Phys. Rev. Lett., 72 (1994), pp. 2797–2800.
[44] W. N. Reynolds, S. Ponce-Dawson, and J. E. Pearson, *Self-replicating spots in reaction-diffusion systems*, Phys. Rev. E, 56 (1997), pp. 185–198.
[45] C. Robinson, *Sustained resonance for a nonlinear system with slowly varying coefficients*, SIAM J. Math. Anal., 14 (1983), pp. 847–860.
[46] J. B. van den Berg, *personal communication*, Free University of Amsterdam, Amsterdam, The Netherlands, 2002.
[47] D. Walgraef, *Spatio-Temporal Pattern Formation: With Examples from Physics, Chemistry, and Material Science*, Springer-Verlag, New York, 1997.
[48] J. Wei, *On single interior spike solutions of the Gierer-Meinhardt system: Uniqueness and spectrum estimates*, European J. Appl. Math., 10 (1999), pp. 353–378.
[49] H. Weinberger, *An example of blowup produced by equal diffusions*, J. Differential Equations, 154 (1999), pp. 225–237.